Laboratory Note 1

Phys 372 Intermediate Lab (Photons)

Energy Dispersive X-ray Spectroscopy (EDXS)

Instructor: Prof. Chen

Winter 2012

SEM Start Up/Shut Down Procedure

START UP :

1. INSTALL SAMPLE: Press "VENT". Use the "SELECT CHECK" button on the console to scroll to "VAC". When "VAC" reads "0" open the sample chamber by pulling gently. Install sample(using conductive adhesive if necessary).
2. PUMP DOWN: Press "EVAC" watching green status display under the monitor and wait until "VAC" reads "100%".
3. CHECK OPERATING
   PARAMETERS: magnification > 10,000
   high voltage > 5kV
4. Push "HT" button on and use "SELECT CHECK" to scroll to "μA"
5. SWITCH to "TV" display mode
6. SLOWLY increase filament current: Slowly turn the filament knob clockwise until the current reading is approx. 80-82μA. Also the "counts" should be present on the monitor.
7. NEVER INCREASE THE ACC VOLTAGE WITHOUT TURNING DOWN L.C. WITH THE BIAS OR FILAMENT CONTROL

SHUT DOWN

1. Turn filament current down SLOWLY: Slowly turn the filament know counterclockwise until the reading in min.
2. SET OPERATING
   PARAMETERS: magnification > 10,000
   high voltage > 5kV
3. Push "HT" button OFF
4. Wait for 2 minutes for filament to cool.
5. Press "VENT" and remove sample only when the "VAC" reading shows "0%"
6. Pump down by pressing "EVAC"
7. Complete and sign entry in the log book.

EDXS Usage Instructions

The EDXS software was created in Labview and performs data acquisition and rudimentary analysis via the XIA Saturn pulse processor.

I – Start the program via the EDXS icon on the desktop. Be sure that the XIA box is on. ~~If the Status indicator is red, turn the box off and then back on again.~~ You will be prompted to initialize the DXP. If this is skipped, you will not be able to acquire data until restarting the program.

II – Acquisition: Start Run under the Acquire pulldown. The run parameters will be displayed above the graph. All data is updated once per second. Adjust Load Current, Spot Size, or Working Distance to bring the Dead Time to an acceptable level. The DSP parameters are currently set to give a good trade-off between low energy sensitivity and high energy resolution. At these settings, the optimal Incoming Count Rate is 3-5 kilocounts (kC) / s. Above this rate your dead time will be very high. Note that Count rate and dead time are averaged over some time frame, so it is sometimes advantageous to Stop Run and start again to get current values.

III – Run types: Preset Run is not yet implemented.

IV – Data format: Data files are stored as tab-delimited text, with a one line header giving run parameters.

V – Element ID: Click on the up or down arrows on the KLM Marker to show x-ray lines for a given element. The + / - keys on the numeric keypad do the same. You can also enter the atomic # (2 digits) to display the lines for that element. CTRL-K (or the Analyze->KLM Markers->Make Persistent menu selection) will cause the x-ray lines for the current element to remain on screen, allowing you to show expected peaks for multiple elements. CTRL-SHIFT-K (or menu selection) deletes markers.

VI – Printing and Peak Labeling: Labeling is not yet implemented. The KLM Markers are not printed, only the raw data.

VII – The graph display:

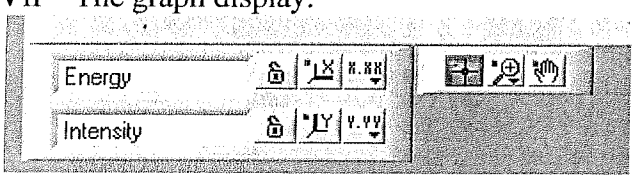

The X and Y Axis buttons will autoscale. The Y.YY button will allow you to change between log(default) and linear scales. The Crosshair button (selected at left) means that mouse activity inside the plot area will control the cursors. The Zoom Tool button drops down to display six zoom options. Most useful are the axis-specific "zoom to selection" tools.

VIII – The cursors:

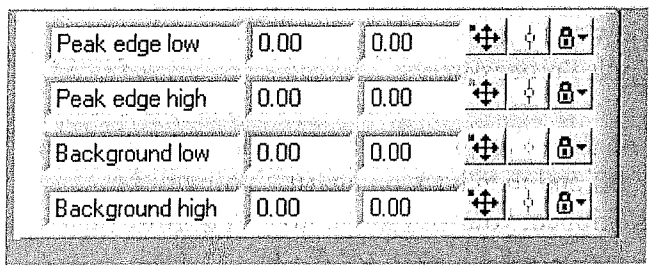

Left Click the center button and select "Bring to Center" for any cursor. The cursor names can be changed, but are so named for the peak area determination (below).

IX – Analyze->Find Peak Area: The background radiation at higher energies can be approximated as a straight line. Given well separated x-ray peaks for multiple elements, relative concentration is proportional to the area under these peaks (preferably the K-a peaks). Place the first two cursors at the peak edges and the second two cursors on the background to either side of the peak. The background points are averaged over 5 neighboring data points, the straight line subtracted, and area under the resulting peak is found and displayed in the Peak Info box.

X – Window transmittance: The x-ray detector is a Moxtek AP1.7, Lithium-drifted Silicon (Si-Li) with a polymer window.

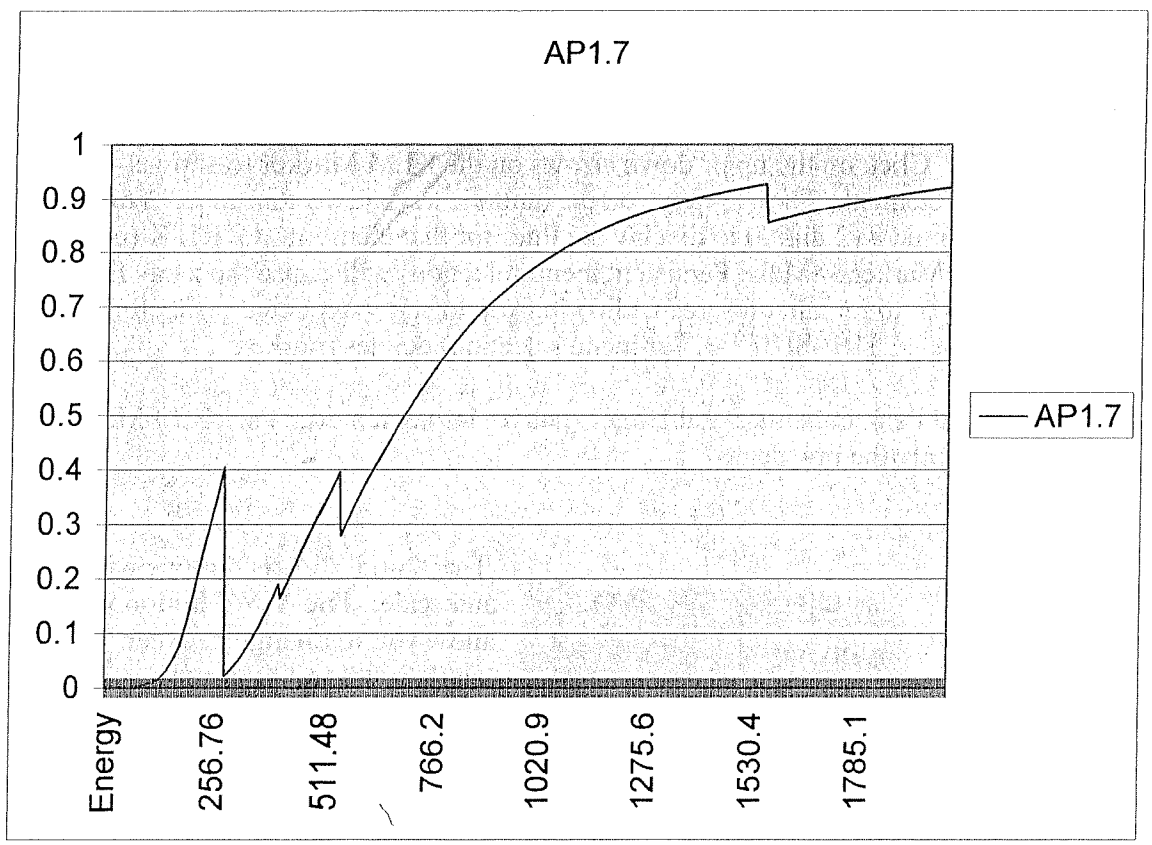

CHAPTER 2 MICROSCOPE DESCRIPTION

2.1 Names of Main Components

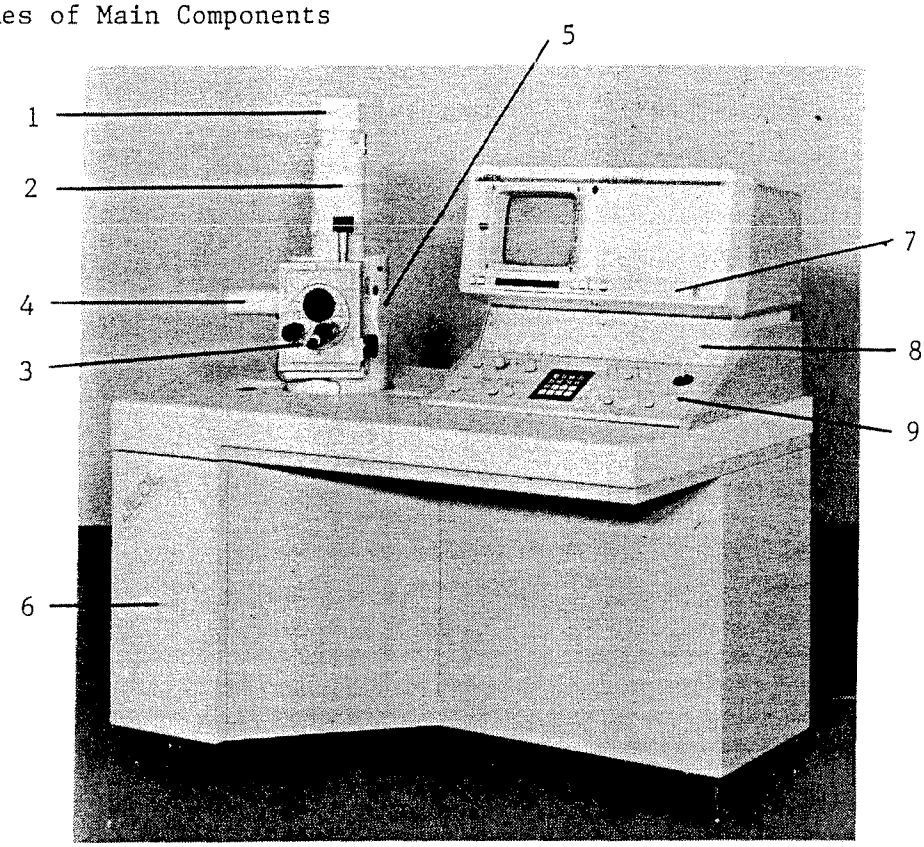

Fig. 2-1 Main Components

1	Electron gun	:	Filament is attached.
2	Column	:	Electron optical system (include anode, condenser lens, objective lens and deflector coil, etc.)
3	Specimen chamber /Specimen stage	:	Specimen mounting·movement (with X, Y, R and T controls)
4	Detector	:	Detects secondary electrons and backscattered electrons.

5 Attachment installation port:
2 ports are provided for the following optional detectors.
. Energy dispersive X-ray spectrometer (EDS)
. Backscattered electron detector (BEIS)
. Cathodoluminescence detector (CLD)
. Infrared cathodoluminescence detector (CLDIR), etc.

6	Cabinet	:	Keeps specimen mounts, tools, instruction manual, etc.
7	Display panel	:	Displays the viewing image, photographing image and operation conditions.
8	Attachment housing	:	Houses optional devices.
9	Control panel	:	Controls and switches are provided.

2.2 Specimen Stage

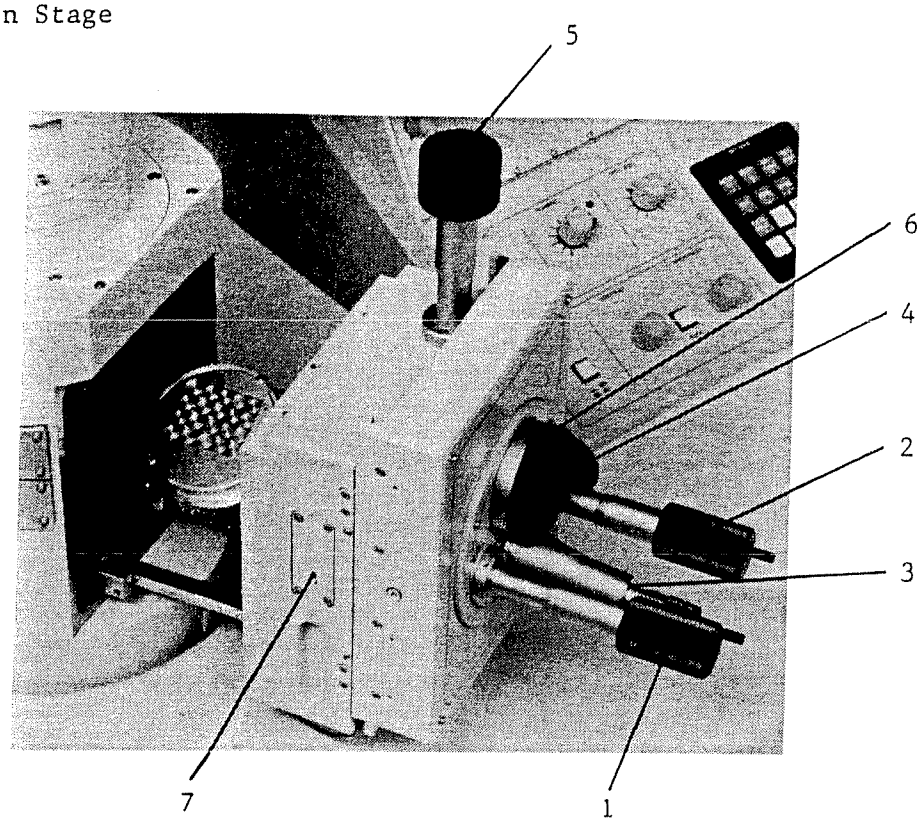

Fig. 2-2 Specimen Stage

1	X control	:	Moves the specimen in front/rear directions as seen from the specimen stage front.
2	Y control	:	Moves the specimen in right/left directions as seen from the specimen stage front. (within an inclined plane at the time of tilt.)
3	R control	:	Rotates the specimen.
4	T control	:	Tilts the specimen when the whole specimen stage is tilted.
5	Z control	:	Sets up the working distance (WD).
6	Viewing port	:	Window for viewing the specimen (AGS/ALC2 is optionally attachable.)
7	Optional attachment port	:	Connects the signal feed terminal for DMA and LGSHIC.

Option

AGS	:	Additional Goniometer Stage
ALC2	:	Airlock Chamber
DMA	:	Digital Microammeter
LGSHIC	:	Specimen Holder for IC

2.3 Control Panel

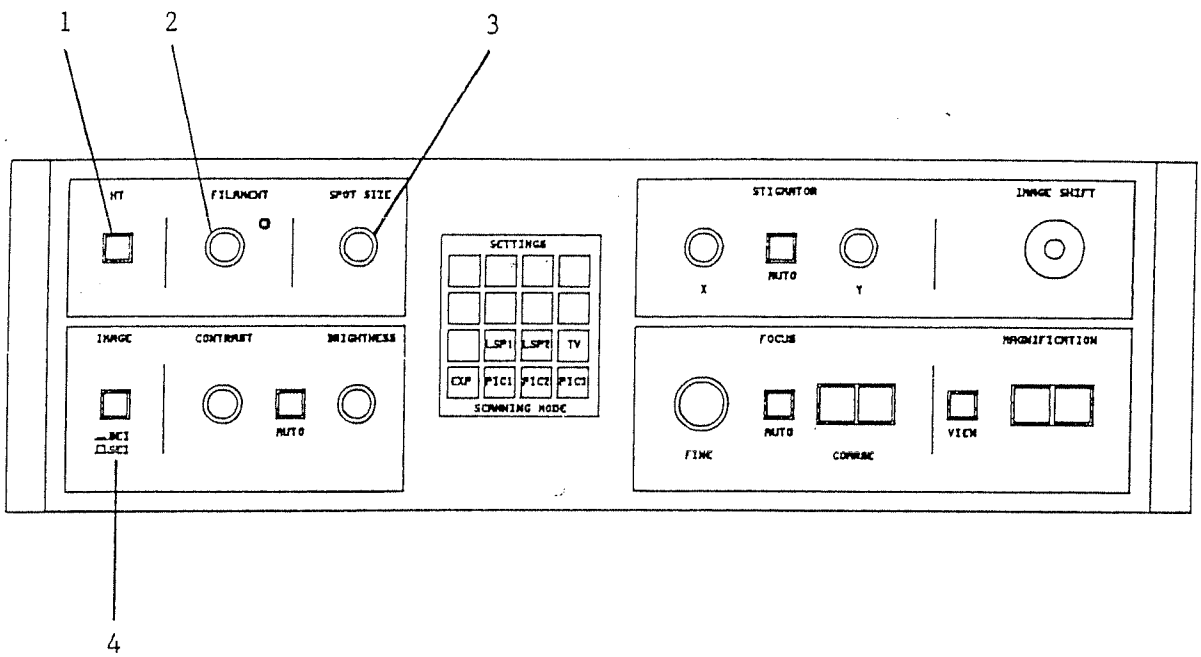

Fig. 2-3a Control Panel

1	HT	:	Accelerating voltage ON/OFF switch (LED lights at ON: RED)
2	FILAMENT	:	Electron gun filament heating current control knob (with stopper)
	Filament monitor lamp	:	The lamp lights if FILAMENT control is set at a position beyond 11 o'clock. If it does not light, the filament is burnt out. (Lamp lights: YELLOW)
3	SPOT SIZE	:	Electron probe diameter and intensity control knob
4	IMAGE SEI/BEI	:	Detector mode selector
	SEI	:	Secondary electron image
	BEI	:	Backscattered electron image (LED lights at ON: GREEN)

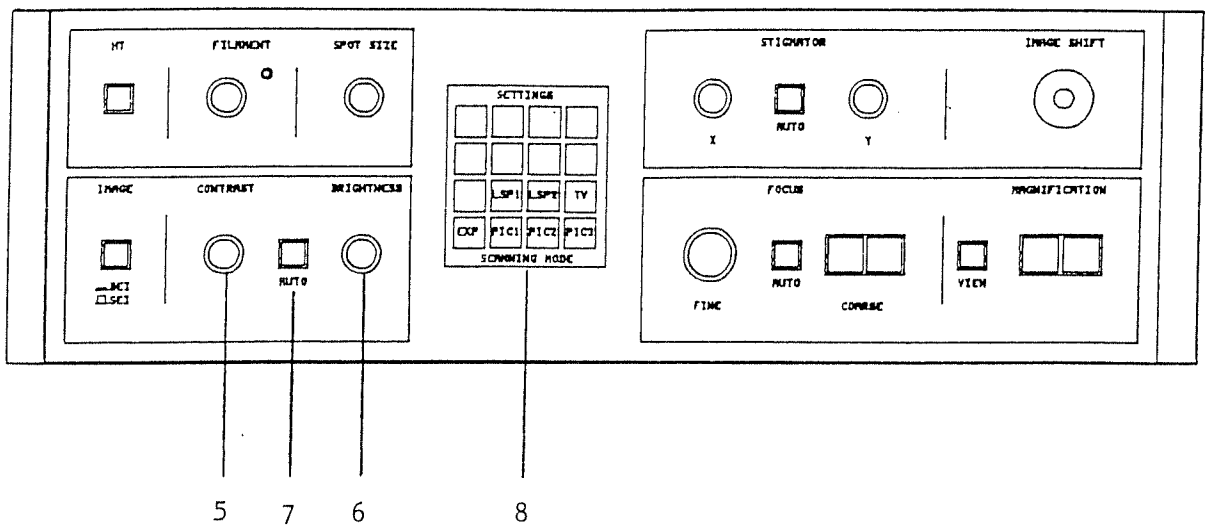

Fig. 2-3b Control Panel

5 [CONTRAST] : Contrast control knob

6 [BRIGHTNESS] : Brightness control knob

7 [AUTO] : Automatic Contrast and Brightness Control (ACB) start switch.
(LED lights at ON: YELLOW)

8 Flat panel key (Keypad)

[SETTINGS] : Accelerating voltage/working distance/memory functions/film data setting

[SCANNING MODE] : Scanning mode/speed setting

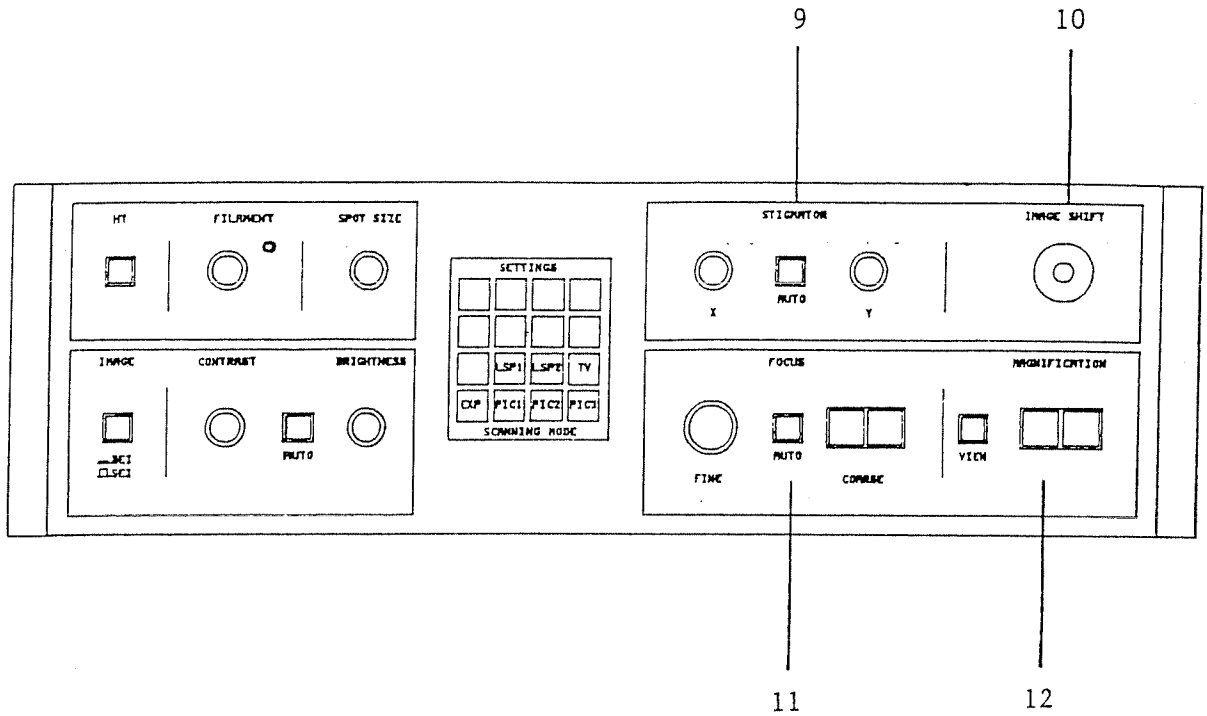

Fig. 2-3c Control Panel

9	STIGMATOR	:	Astigmatism correction knob (X·Y)
	AUTO	:	Automatic astigmatism correction device (ASD) start switch (LED lights at ON: YELLOW)
10	IMAGE SHIFT	:	Electromagnetic image fine shift with joystick
11	FOCUS	:	Focusing
	FINE	:	Focus fine control
	COARSE	:	Focus coarse switch (Left: Down, Right: Up) Buzzes at MIN/MAX.
	AUTO	:	Automatic Focusing Device (AFD) start switch (LED Lights at ON: YELLOW)
12	MAGNIFICATION	:	Magnification selection switch (Left: Down, Right: Up)
	VIEW	:	Preset magnification ON/OFF switch (LED Lights at ON: YELLOW)

2.4 Display Panel

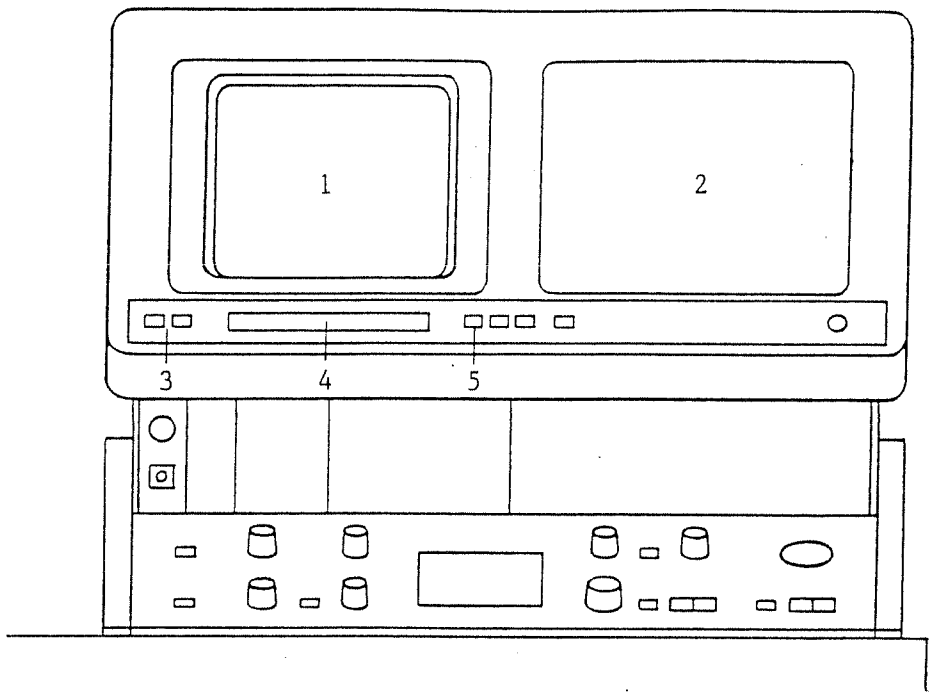

Fig. 2-4a Display Panel

1	Observation CRT	:	9" green CRT for both observation and photography of scanning image
2	Photographing CRT installation space	:	9" short-persistence CRT (PRD1: option) is installed.
3	VACUUM	:	Evacuation operation switch
	VENT	:	Column and specimen chamber reach atmospheric pressure (admit air). (LED lights at VENT: GREEN)
	EVAC	:	Evacuates the column and specimen chamber to vacuum. (LED lights at EVAC: YELLOW)
4	Operation condition display	:	Liquid crystal display (LCD) (A 40 columns × 2 lines; with a back light)
	Upper line	:	Accelerating voltage, working distance, magnification, film number, photographing speed and others are displayed.
	Lower line	:	Evacuation sequence, check data, warning and others are displayed. (This changes into a photo monitor during photography.)
5	CHECK SELECT	:	Check item selection switch

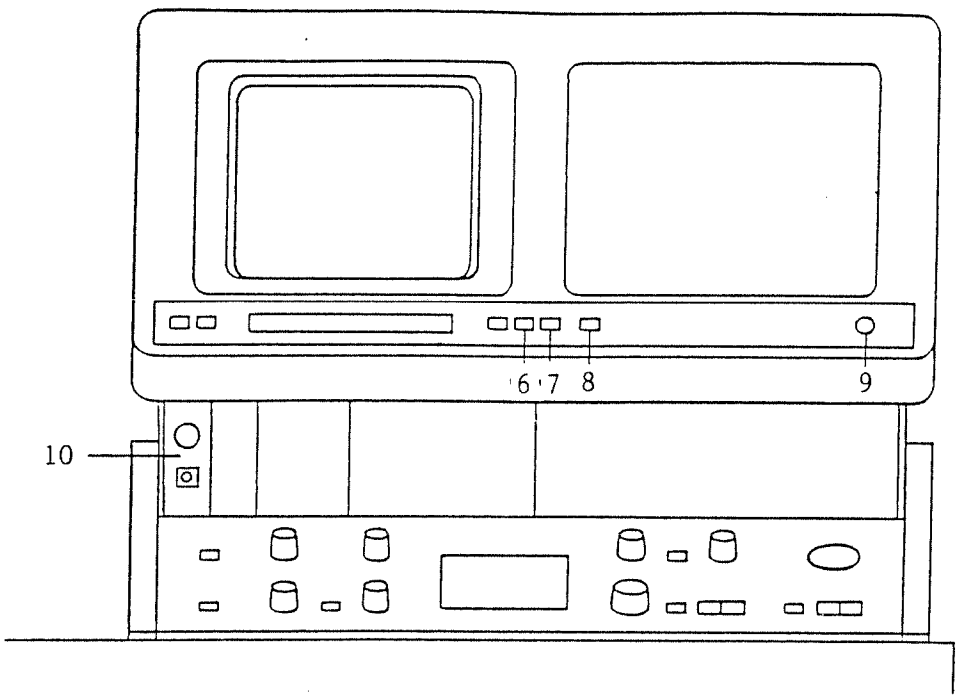

Fig. 2-4b Display Panel

6 [COUNT] : Film number counter ON/OFF switch
(At ON, 2 digits at the right of film number automatically count at each photographing.)

7 [PHOTO SPEED] : Photographing speed selection switch

> : For normal photographing: 86.4 sec (50 Hz)/72 sec (60 Hz)

>> : For quick photographing: 28.8 sec (50 Hz)/24 sec (60 Hz)

Mark (> or >>) is displayed at the right edge of upper line in LCD.

8 [SHUTTER] : Automatic shutter
(LED lights at ON: GREEN)
The remaining photographing times are displayed at the right edge of lower line in LCD.

9 [POWER] : Power key switch/CPU reset switch

Start up: [OFF] → [START] → [ON]

Shut down: [ON] → [OFF]

CPU reset: [ON] → [START]

10 [DFU] : Dynamic Focusing Device (DFU)
Correct the focus in tilting specimen

2.5 Rear Panel

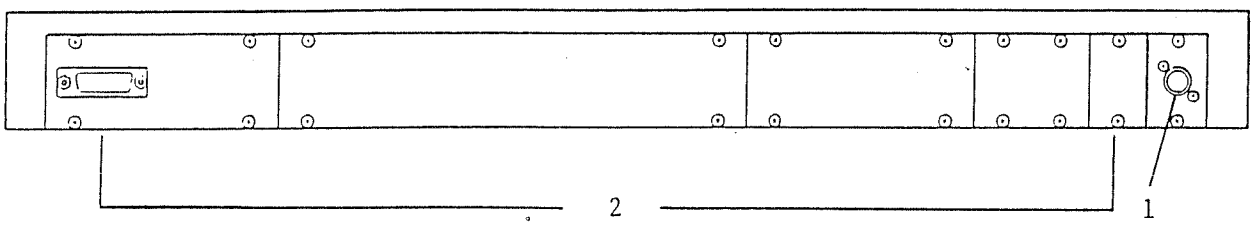

Fig. 2-5 Rear Panel

1 TV signal output terminal (BNC-R connector)
2 Connector port for several attachments

CHAPTER 3 OPERATION

CONTENTS

CHAPTER 3 OPERATION

3.1 Outline of Operating Procedure

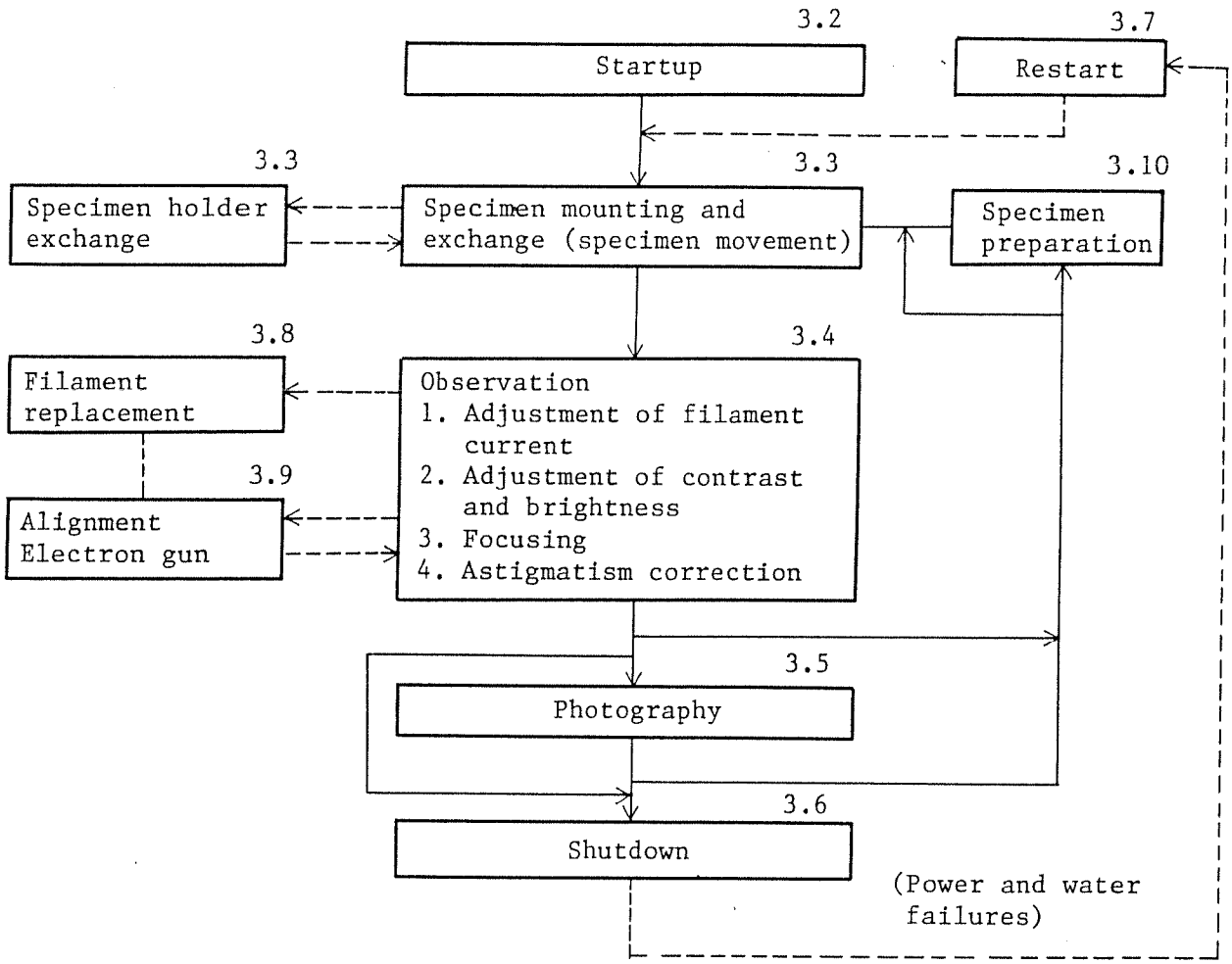

Fig. 3-1 Operating Procedure

——— routine operation

- - - - - as required

Notes: 1. When mounting the Camera for Scanning Image (CSI), be sure to install it prior to startup.

2. When mounting the attachments (especially for mounting and exchanging the specimen), refer to the respective instruction manuals for them.

3.2 Startup

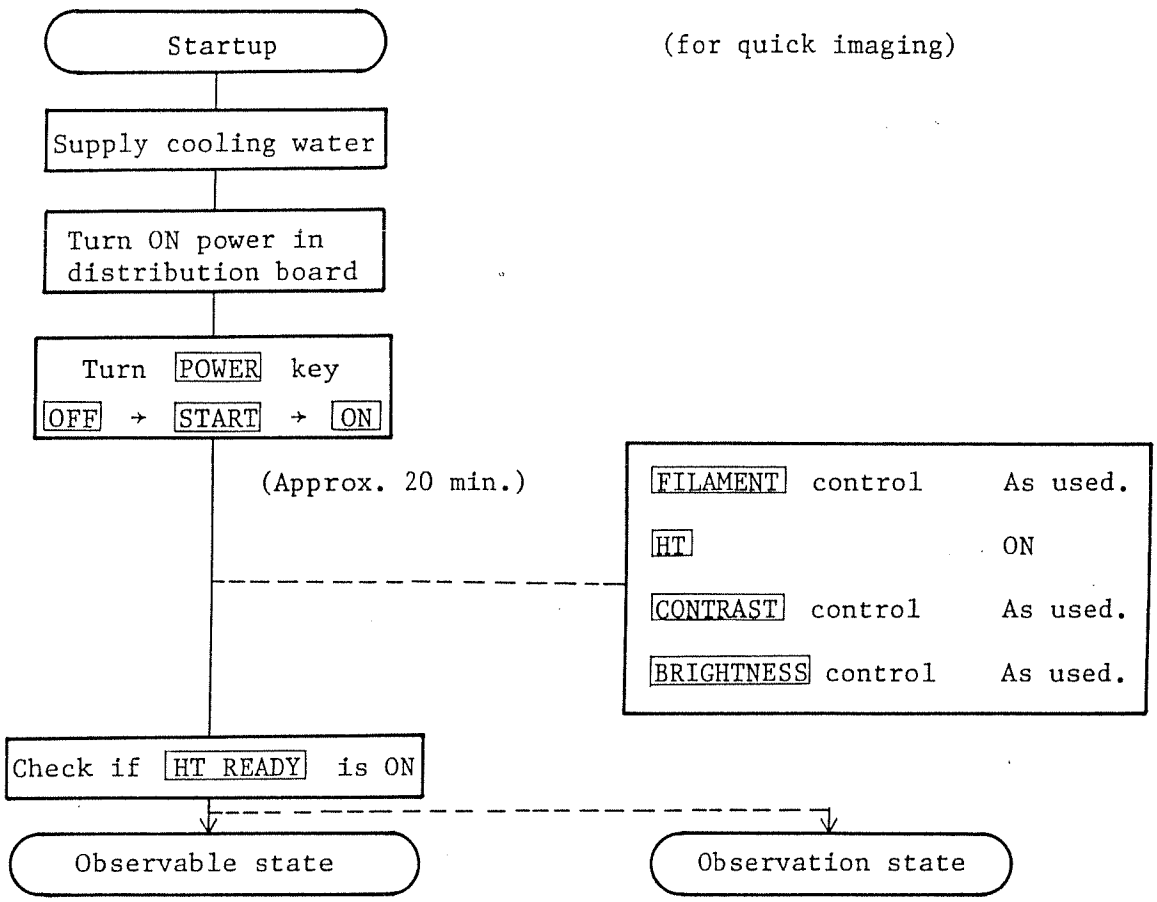

1. Turn on the tap to supply cooling water. Set the flow rate to around 1.5 to 2 ℓ/min.
   Note: The flow rate exceeding 2 ℓ/min may cause excessive cooling of the oil diffusion pump (DP) or vibration.
2. Turn ON the distribution board switch and insert the key into the POWER switch located at the right-hand bottom of the display panel. Turn the key fully to the START and release it (returns to ON.) The DP WAIT sequence indicator on Liquid Crystal Display (LCD) lights up and the oil rotary pump starts to rotate.
3. The microscope is automatically evacuated and the HT READY sequence indicator on LCD light up in approx. 20 min to make observation possible.

4. Initial settings of switches and controls

[IMAGE] [SEI/BEI] switch	:	[SEI] (LED goes out.)
[HT] switch	:	ON (Red LED lights up.)
[FILAMENT] control	:	As used
[SPOT SIZE] control	:	10 to 12 o'clock position
[CONTRAST] control	:	As used
[BRIGHTNESS] control	:	As used

5. Push SCANNING MODE [TV] or [PIC1] and press AFD and ACB [AUTO] start switches in that order after completion of their respective operations (after image appears.)

Goerg H. Michler

Electron Microscopy of Polymers

With contributions by
Dr. R. Godehardt · Dr. R. Adhikari · Dr. G.-M. Kim
Dr. S. Henning · DP V. Seydewitz · DP W. Lebek

Springer

4 Scanning Electron Microscopy (SEM)

Today, scanning electron microscopy (SEM) is a versatile technique used in many industrial labs, as well as for research and development. Due to its high lateral resolution, its great depth of focus and its facility for X-ray microanalysis, SEM is often used in materials science – including polymer science – to elucidate the microscopic structure or to differentiate several phases from each other.

After a brief historic overview, this chapter explains the assembly and the mode of operation of SEM, which deviates from standard microscopes. This includes descriptions of the fundamentals of electron optics, the electron optical column, and the physical basics of electron–specimen interactions, which aid the understanding of contrast formation and charging effects. Because it is important to know the factors that influence X-ray microanalysis, a separate section about the origins of X-ray spectra and their interpretation has also been added. A discussion of environmental scanning electron microscopy (ESEM™) – a special development of SEM that is particularly useful when nonconducting or "wet" samples are to be examined – completes the chapter.

4.1 A Brief History of SEM

Parallel to the development of the transmission electron microscope (Sect. 2.1), Max Knoll had the idea of developing an electron microscope for investigating compact or bulk samples, and he demonstrated the basic principle for a scanning electron imaging device using two Braun-type cathode ray tubes in 1935 [1]. In both of these tubes, the electron beam is scanned by a pair of magnetic coils. In one of them, a plate with different surface layers was irradiated with a scanning beam, and the emitted secondary electrons that reached the anode were collected. The signal obtained was used to control the local brightness of the beam in the second tube. The surface layers of the irradiated plate could therefore be visualised by the second tube. This experiment was a proof of the material-specific dependence of secondary electron emission, but it was still not adequate for microscopic imaging.

Manfred von Ardenne developed an electron probe microscope in 1938 that used electron-optical lenses to focus the beam. This idea originated from the fact that resolution-limiting chromatic failures do not play a role in such a microscope [2–4]. He presented this instrument, in which electrostatic scanning plates were applied to a TEM, only a few years after Knoll's and Ruska's first TEM. This type of microscope is

now known as a scanning transmission electron microscope (STEM). However, Ardenne's prototype fulfilled the minimum criteria for a scanning electron microscope (SEM) from today's point of view. The first scanning electron microscope of the usual type was described and developed by Zworykin et al. [5] in 1942 using three electrostatic lenses and electromagnetic coils between the second and third lenses.

Unfortunately there was no further development in the field of SEM in Germany, and Ardenne's instruments were lost in 1944 in an air raid during World War II. In the latter half of the 1940s, Charles Oatley continued research into SEM at Cambridge University, but it was still quite some time until the first commercial SEM was made available. One of his graduate students, McMullan, enhanced the instrument of Zworykin in order to achieve a lateral resolution of about 50 nm [6]. Smith [7] replaced the electrostatic lenses by electromagnetic ones and introduced a double deflection system to correct astigmatism. At the beginning of the 1960s, Everhardt and Thornley [8] improved the secondary electron detector by adding a light pipe between the scintillator and multiplier. All these improvements provided a great impetus for the development of the first commercial scanning electron microscope, which was named Stereoscan Mark 1 and sold by Cambridge Instruments in 1965.

Parallel to the Cambridge group, Coslett's group at the Cavendish Laboratory combined the X-ray analytical capability of Castaing's "microsonde electronique" (electron microprobe) [9] with an imaging facility and developed the scanning electron probe X-ray microanalyser [10]. From the middle of the 1960s until the present several improvements in electron generation and electron optics have been made that have enhanced the resolution power. At the end of the 1980s, computerised SEM entered the scene, which led to the introduction of the digital scanning generator for digital image recording and processing.

At that time a new type of SEM with a vacuum of some tens of mbar in the specimen chamber was developed. One reason for this development was the idea of directly preventing the charging of insulating samples; another reason was to make it possible to investigate humid samples. Because of the high-voltage flashovers of the Everhardt-Thornley detectors normally used, most instruments only allow imaging with backscattered electrons in the low vacuum mode. Danilatos provided a completely new principle, the "gaseous secondary electron detector" (GSED) [11]. Using this type of detector and subsequent developments from Danilatos [12–14], the newly formed ElectroScan Corporation produced the first "environmental scanning electron microscope" (ESEM™) in 1989, which was based on electron optics from Philips Eindhoven that had the ability to image with secondary electrons. After the acquisition of ElectroScan in 1996 by Philips/FEI, a new generation of ESEMs came onto the market. The special features of this instrument are explained in Sect. 4.6.

4.2 Fundamentals of Electron Optics and Signal Generation

4.2.1 Principle of SEM

The basic principle of the SEM [15–17] is based on Knoll's experiment [1] and von Ardenne's idea for a scanning probe transmission microscope [4].

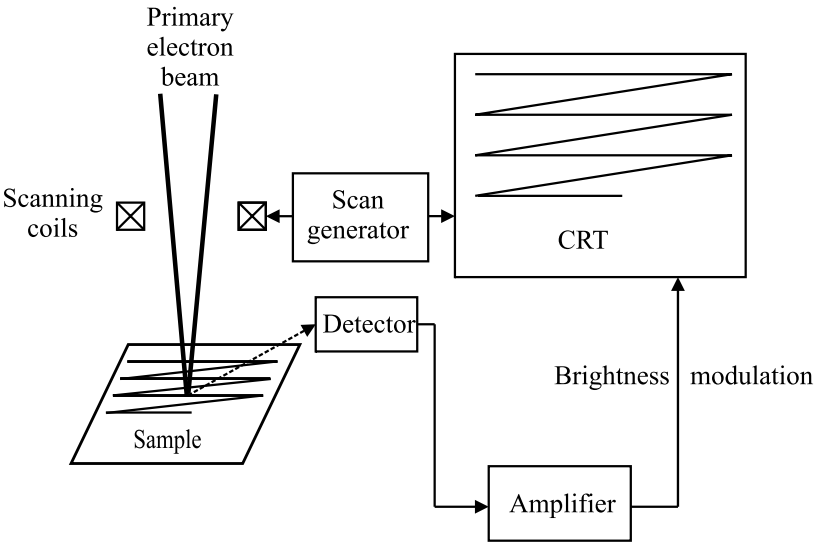

Fig. 4.1. Scheme showing the principle of SEM

In a similar process to the scanning of the electron beam in a cathode ray tube (CRT), the focussed electron beam scans line by line over the surface of the specimen in the evacuated microscope column and forms signals based on the interactions between the beam and the sample, which are electronically detected and amplified by suitable equipment. Originally, the response signal was displayed as a brightness modulation on a CRT where the electron beam is driven simultaneously to the beam in the column, as illustrated in Fig. 4.1. Nowadays, digital computer techniques have replaced the traditional CRTs. As the area of the displayed image remains unchanged, the magnification of the image is determined by the dimension of the scanned sample area (see Sect. 4.3.4). Generally, the resolution of the SEM image is determined both by the diameter of the electron probe focussed on the sample surface (see Sect. 4.2.2) and the interaction of the primary electrons (PE) with the sample (see Sect. 4.2.5).

4.2.2 The Lateral Resolution Power of SEM

Using the electron-optical system within the SEM column, the electron beam created by the electron gun (see Sect. 2.3.1) is reduced to a sufficient diameter to form a very fine focussed electron probe. The PE beam diameter in the electron gun depends on the type of cathode (respective gun type) and is formed by the first crossover of the electron trajectories (see Fig. 2.7d). The first crossover generated from the tungsten cathode must be scaled down to approximately a factor of 1000 to attain a reasonable resolution. Two or three (although sometimes more) electromagnetic lenses are needed to demagnify the beam diameter (see Fig. 4.2). Furthermore, the first lens or the first and second lenses (called condenser lenses) are used to vary the PE beam current.

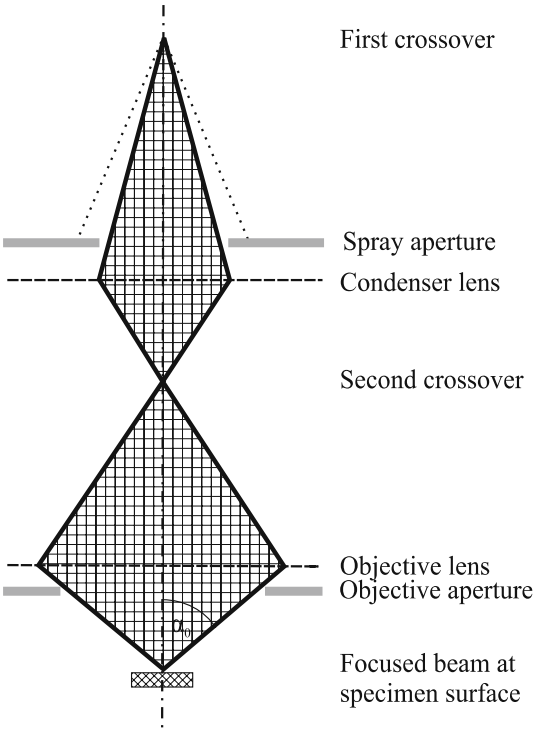

Fig. 4.2. Scheme of the electron-optical relationship in SEM

The minimal achievable diameter d_0 of the beam can be estimated with the help of the lens law (see Eqs. 2.8 and 2.9). Another quantity used to characterise the electron beam performance is the gun brightness R, defined by

$$R = \frac{j_c}{\pi\alpha_c^2} = \frac{j_o}{\pi\alpha_0^2} = const. \tag{4.1}$$

where j_c is the beam current density at crossover, α_c is the aperture angle at crossover, j_0 is the beam current density at the specimen surface and α_0 is the aperture angle at the specimen.

The aperture angle α_0 is determined by the ratio of the diameter of the last diaphragm r to the working distance L, which is the distance between the pole piece of the objective lens and the specimen:

$$\alpha_0 = \frac{r}{L}\,. \tag{4.2}$$

A homogeneous beam density within the beam diameter d_0 at the sample surface corresponds to the following beam current I_0:

$$I_0 = \frac{\pi}{4} d_0^2 j_0\,. \tag{4.3}$$

Combining Eqs. 4.1 and 4.3 results in

$$I_0 = \frac{\pi^2}{4} R d_0^2 \alpha_0^2 \tag{4.4}$$

and

$$d_0 = \left(\frac{4 I_0}{\pi^2 R} \right)^{1/2} \frac{1}{\alpha_0} = \frac{C_0}{\alpha_0} . \tag{4.5}$$

This equation is also valid when the homogeneous illumination is replaced with a Gaussian-distributed one. In this (more realistic) case, d_0 corresponds to the half-width of the full maximum (HWFM) of the distribution.

It can be seen from Eq. 4.5 that the diameter of beam is directly proportional to the beam current and indirectly proportional to gun brightness and aperture angle. In reality, the effective diameter of the beam d_b at the specimen is somewhat larger due to aberrations (see Sect. 2.2.3).

An acceptable signal-to-noise ratio in the secondary electron signal (see Sect. 4.3.3) usually requires a minimum beam current I_0 of between 10^{-12} A and 10^{-11} A. Figure 4.3 shows the dependence of d_b on the aperture angle and the beam current for a tungsten filament gun.

The figure also shows that there is an optimum value for the aperture angle as a function of the beam current. The gun brightness R of the Schottky emitter or field-emission guns (FEG) is higher than that of the tungsten or LaB_6 cathodes (see Table 2.4). According to Eq. 4.5, a much lower beam diameter is achieved at the same beam current with the FEG rather than thermionic guns. Thus, if an FEG is used, a resolution power of 2 nm or even less can be achieved.

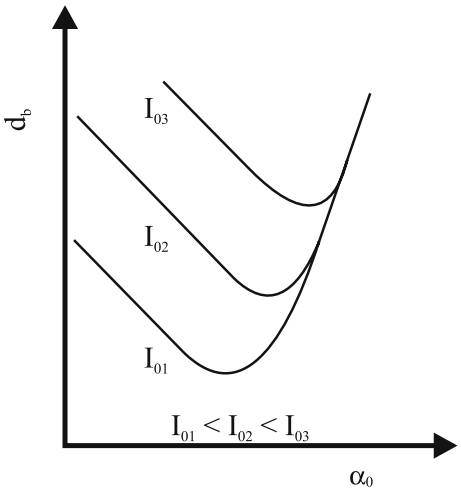

Fig. 4.3. Dependence of the effective beam diameter d_b (in the nm range) on the aperture angle a_0 (in the mrad range) and the beam current I_0 for a tungsten filament gun (schematic, after [15])

4.2.3 Comparison of Various Cathode Types

The types of cathodes (usually termed "guns") frequently used in an electron microscope have been already described (in Sect. 2.3.1 and Table 2.4). To select the most appropriate gun type, the operator should take into account first the minimum resolution power (Sect. 4.2.2) required for the investigations and secondly all of the other parameters of cathodes. Table 2.4 shows the main differences between tungsten and LaB_6 cathodes and the FEG. While the beam diameter increases with increasing probe current for the first two types, in the case of FEG there is a probe current interval where the beam diameter stays constant with increasing probe current. The most important feature of the gun for the user of an SEM is the available probe current of the emitters. For certain SEM techniques, like WDX analysis (see Sect. 4.5.6) or cathodoluminescence, thermionic emitters have been preferred in the past. Nowadays thermal FEG is a good compromise. This emitter type offers on the one hand a good resolution in the SE mode and on the other hand sufficient probe current for the application techniques mentioned before.

4.2.4 Depth of Focus

The depth of focus is one of the outstanding features of SEM. While the depth of focus of a light microscope for a magnification of about 200× is in the µm region, the depth of focus of the SEM at same magnification covers mm.

The depth of focus is a function of both the convergence angle α_0 of the electron beam and the magnification M (Fig. 4.4). Noting that $\tan \alpha_0 \approx \alpha_0$ at $\alpha_0 \ll 1$, the focus depth S is expressed by:

$$S = \frac{2r}{\alpha_0} = \frac{0.1\,\text{mm}}{\alpha_0 \cdot M}\,. \tag{4.6}$$

Here, $2r$ is the beam diameter which produces a corresponding spot on the display which can just about be resolved by the human eye (ca. 0.1 mm). Equation 4.6 reveals that the depth of focus decreases with increasing magnification and aperture angle α_0. The facet eye of a fly (see Fig. 4.5) demonstrates high depth focus in SEM imaging.

4.2.5 Interaction of Primary Electrons with Sample

Signal generation in SEM is a result of the interaction between the incident electron beam and a thin surface layer of the sample, which depends on the beam energy. The primary electrons are charged particles and so they interact strongly with the electrically charged particles of the atoms in the sample, i.e. both with negatively charged electron clouds and positively charged nuclei. The interaction is said to be *inelastic* if some of the energy of the primary electron is lost during the interaction. If no energy is lost the interaction is said to be *elastic*. The fundamentals and applications of these scattering processes are also described in Sects. 2.4.1 and 3.9.

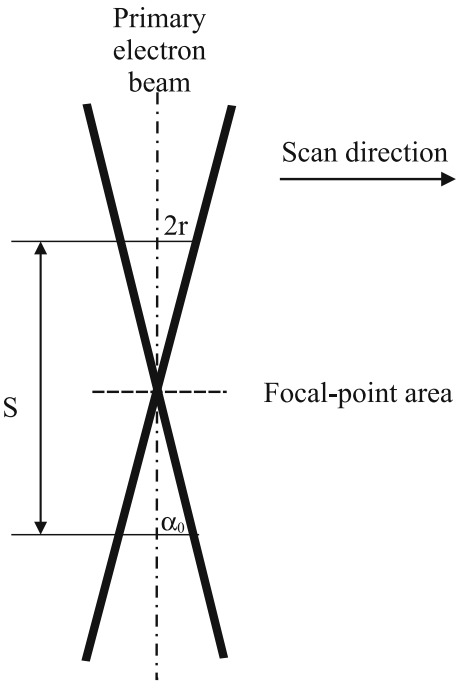

Fig. 4.4. Scheme of the derivation of depth of focus in SEM (after [15])

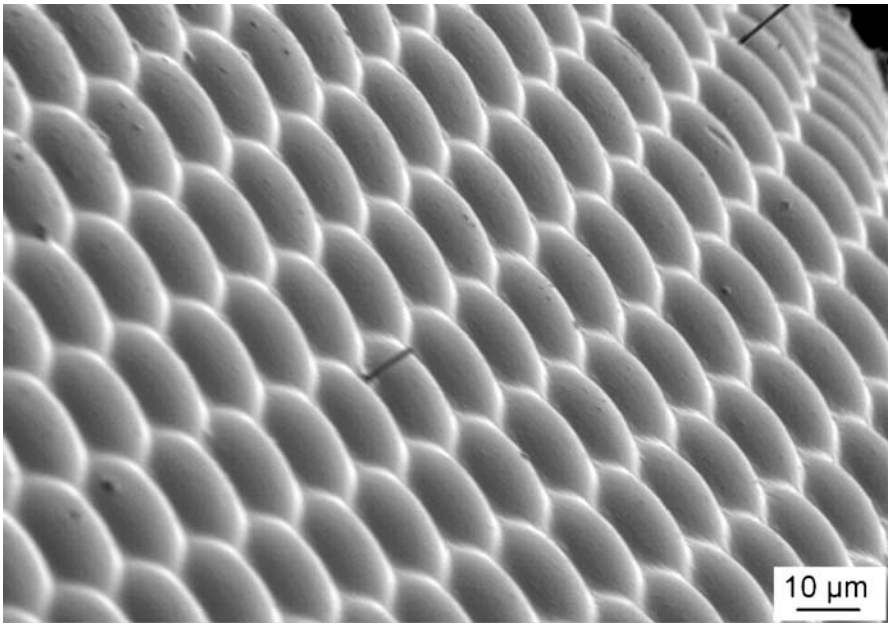

Fig. 4.5. SE micrograph of the facet eye of a fly showing a high depth of focus

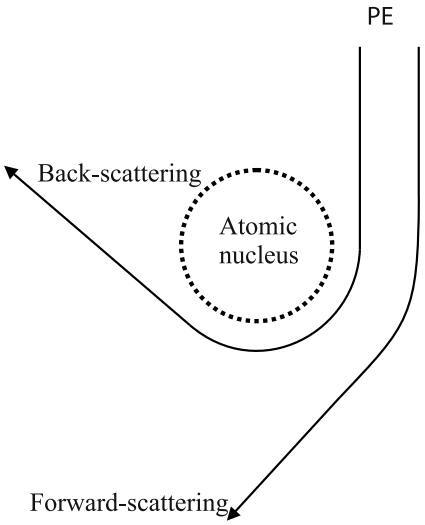

Fig. 4.6. Rutherford scattering of a primary electron in the Coulomb field of an atomic nucleus

PE/Nucleus Interaction

When electrons enter the electric field of an atomic nucleus, which can be partly screened by electron clouds, their paths are deflected. Generally, this so-called Rutherford scattering results in parabolic PE trajectories. The larger the atomic number of the atoms in the interaction region and the smaller the distance between the nucleus and the PE, the stronger the deflections of the latter and hence the more curved PE paths.

While contrast-forming interaction processes in a TEM are restricted to weak scattering events with small scattering angles (forward scattering), electron scattering in bulk samples in SEM also includes a high proportion of strong scattering events where the directions of the PE trajectories are significantly changed, with some even sent back along their original paths (back scattering), as illustrated in Fig. 4.6. While a negligible amount of energy is lost due to conversion into X-ray continuum radiation ("bremsstrahlung"; see Sect. 4.5.1), the interactions are assumed to be elastic. Electrons that undergo one or more Rutherford processes and leave the sample surface without notable energy loss are called backscattered electrons (BSE).

PE/Electron Cloud Interaction

PEs striking the sample surface may also interact with the electrons of atoms within the surface region. Owing to their equivalent masses and identical charges, the interaction is inelastic. If the energy of the incident electron is high enough, the valence electrons of the surface atoms can easily be released from the atoms (Fig. 4.7). These electrons are called secondary electrons (SE). Their kinetic energies are very low (only a few electron volts), just enough to surmount the work function of the sample. However, only SE originating from a very thin surface layer a few nm in thickness can contribute to the detectable signal, as all of the SEs generated in deeper regions of bulk samples will recombine. Generally, ionised or excited atoms will rapidly con-

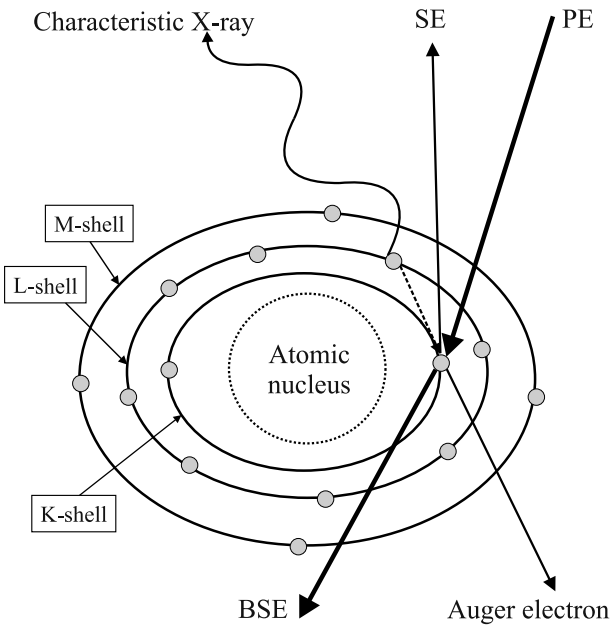

Fig. 4.7. Inelastic interaction between primary electrons and electrons in atomic shells

vert back to their initial states. These processes are accompanied by the emission of characteristic X-rays (see Sect. 4.5.1) or Auger electrons, which is the basis for analytical investigations by means of SEM.

4.3 The Instrumentation of SEM

4.3.1 The Column

Generation of the Focussed Electron Beam

As already described in Sect. 4.2.1, the SEM consists of a column (which is a unit containing the lens system that forms the finely focussed electron beam), a specimen chamber, detectors, as well as imaging and recording units (see Fig. 4.1).

The typical acceleration voltage range of SEM lies between some hundreds volts and 30 or 35 kV. PEs originating from the virtual source at the first crossover (in the electron gun) as a divergent beam pass through the anode aperture and enter the lens system of the SEM. Usually, a spray aperture is placed in the entrance plane of the lens system to block electrons moving along paths very far from the optical axis.

The lens system acts on the electron beam in two ways. On the one hand, it transfers the PEs from the gun crossover to the plane of the specimen surface, and in doing this it reduces the beam diameter considerably to form a very fine probe. On the other hand, the beam current must be controlled by the lens system. In principle, a system of just two lenses combined with an aperture diaphragm could be used to do this, as

illustrated in Fig. 4.2. The first lens, called a condenser lens, that has a variable and relatively weak magnetic field (and a correspondingly large focal length) is mainly used to control the beam current, while the second one, called the objective lens, is a short-focal lens (with a strong magnetic field) which is primarily responsible for the demagnification of the beam diameter. However, the condenser lens is usually replaced by a system of condenser lenses that allow the beam current and beam diameter to be varied independently.

The aperture angle α_0 limiting diaphragm is usually placed within the pole piece of the objective lens (see Figs. 4.2 and 4.8). This aperture can usually be adjusted from outside and must be corrected after changing the high voltage and beam current. One should note that the middle points of the images remain unaltered during the focussing operation.

Scanning Unit and Stigmator

Two pairs of scanning coils to deflect the electron beam in the x- and y-directions are located within the objective lens (see Fig. 4.8). These coils are driven by two different sweep signals, where, as in a CRT, the slew rate of the pair of scanning coils for x-deflection is a multiple value of that for the other pair. The increase in the sweep rate over time influences the change in the magnetic field. Due to the change in the magnetic field in the coils, the electron beam will be deflected away from the optical axis and so the beam scans across the sample surface. In the process both of the sweep voltages range from a maximum negative value to the same positive value, so that the middle of the scanned area on the specimen surface occurs along the optical axis.

The higher the maximum sweep voltage, the stronger the magnetic field in the coils and the larger the maximum elongation at the sample. The size of the scanned area on sample surface can be changed by varying this maximum voltage. This procedure controls the magnification of the SEM (Sect. 4.3.4).

As mentioned in Sect. 2.2.3, astigmatism occurs in all electron lenses due to instrumental imperfections introduced during the manufacturing process. In SEM, this astigmatism also leads to a deformation of the ideal spherical cross-section of the electron beam. Due to the deflection of the beam during the scanning process, the beam spot presents an increased elliptical cross-section, in particular at the fringes of the frame. This elliptical distortion leads to loss of resolution and to reduced image

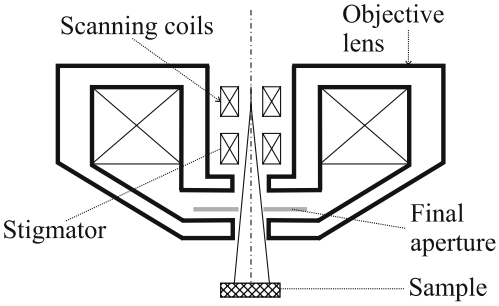

Fig. 4.8. Scheme of an objective lens with scanning coils and stigmator

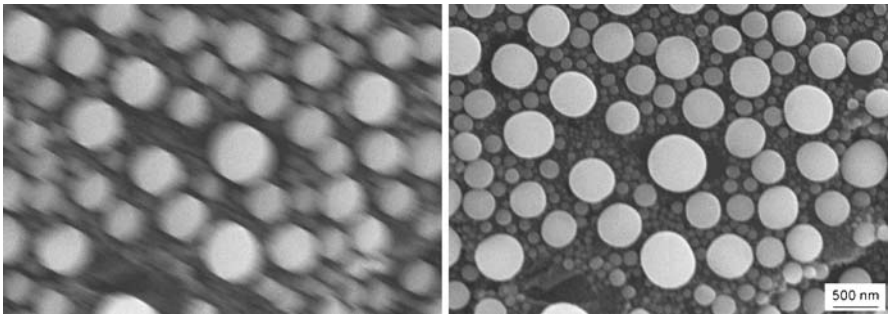

Fig. 4.9. SE image demonstrating the appearance of an elliptical focus due to astigmatism (*left*) and compensated image (*right*) (test sample Au on C)

sharpness. However, the so-called *stigmator* (see Fig. 4.8) can be used to compensate this distortion (Fig. 4.9).

4.3.2 Specimen Chamber and Goniometer

A specimen chamber with a goniometer unit, which enables sample movement to be defined, is attached to the microscopic column below the pole piece of the objective lens. Usually, the goniometer not only enables rotations and translations of the specimen in all (x, y and z) directions, but it also enables the specimen to be tilted. The maximum tilt angle is usually 90° towards the Everhardt-Thornley detector (see below) and 10–30° in the opposite direction. Modern goniometers allow specimen movements of more then 5 cm in the x- and y-directions and a few cm along the z-direction. For a constant deflection of the electron beam, the scanned surface area depends on the distance between the specimen surface and the scanning coils (theorem on intersecting lines), i.e. z-translation is very important when choosing the optimal working distance (WD). In general, WD is defined as the distance between the pole piece of the objective lens and the specimen surface. It should be noted that a higher resolution can be achieved at lower WD. Usually a corresponding decrease in the detected SE signal due to shadowing effects limits the reduction of WD in practice. The use of an optimal WD is of special importance for analytical investigations performed by X-ray microanalysis (Sect. 4.5).

Often the sample is transferred to the specimen support of the goniometer via an airlock; otherwise the chamber and the lower part of the column have to be vented. The specimen support of the goniometer is electrically insulated from the other parts of the microscope. Thus, absorbed electrons can be detected using a special amplifier or a warning signal can be generated using a suitable electronic unit when the specimen collides with the microscope.

It is also possible to incorporate special devices (heating or cooling units, tensile or bending modules, etc.) into the specimen chamber to carry out in situ tests of the sample (see Chap. 6).

4.3.3 Detectors

Secondary Electron Detector

An SEM is normally equipped with an Everhardt-Thornley detector [8] for imaging the sample surface via collected secondary electrons. This detector is a combination of a scintillator and a photomultiplier. Due to its low noise, a photomultiplier is favoured over other kinds of amplifiers used to amplify small currents in the range of nA to pA, which are typical of the emitted SE currents in SEM.

The Everhardt-Thornley detector is based on the following principle.

The secondary electrons that leave the sample possess energies of up to only 50 eV. These low-energy electrons can be collected with high efficiency by a grid electrode that is positively biased with a voltage of about 200 V. The collected SEs are subsequently accelerated toward the scintillator, which is covered with a thin aluminium layer and placed at a voltage of about +10 kV.

The accelerated SEs striking the scintillator possess sufficient energy to emit photons by converting their kinetic energies. The generated photons pass through a light pipe into the photomultiplier, where they cause the emission of photoelectrons. The latter are highly amplified by electron multiplication at the dynodes in the multiplier, and so finally an electronic signal that is proportional to the number of collected SEs is produced (Fig. 4.10).

If the bias voltage of the scintillator electrode switches off or if a negative bias is applied to the collector grid, only highly energetic BSEs can reach the scintillator, which leave the sample and head towards the detector. Due to geometric constraints, the signals from sample locations turned away from the detector do not contribute to the imaging; the resulting BSE image shows shadow phenomena. This mode is generally used as a simple method for BSE imaging. Another BSE detector with a higher detection efficiency is described below.

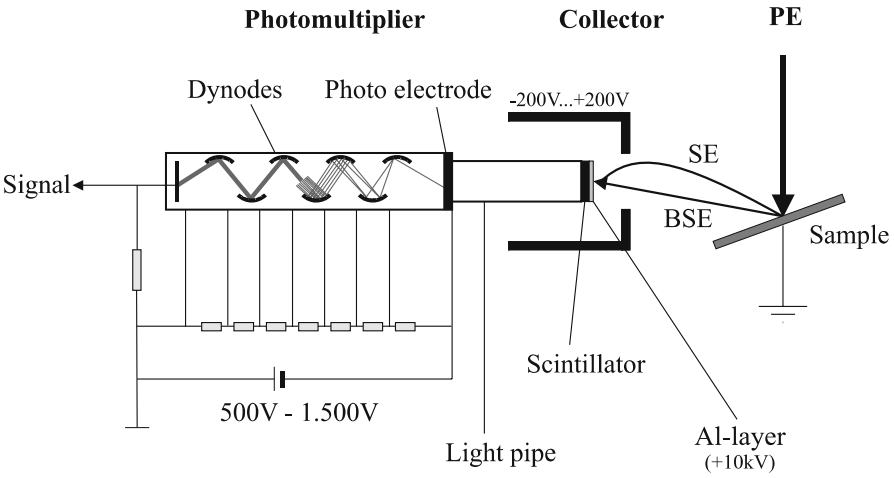

Fig. 4.10. Principle of the Everhardt–Thornley detector

The scintillator material consists of either a layer of fluorescent powder (placed on optically transparent platelets) or an yttrium-aluminium-garnet (YAG) crystal. The first type can degrade due to prolonged bombardment with high-energy electrons and hence need to be replaced at regular intervals.

Other Detectors (Including Solid State Backscattered Electron Detectors)
In addition to the type of detector discussed above, there are a large number of commercially available detectors that can be bought as complementary equipment for SEM. However, most of these are rarely used in polymer research. Only a few of them have found application in special electron microscopic tests, such as BSE detectors based on the electron voltaic effect in a solid state detector, and energy dispersive X-ray detectors, which will be discussed in Sect. 4.5.3.

The backscattered electron detector consists of two or four semiconductor diodes which are symmetrically arranged around the opening of the pole piece of the objective lens. In these diodes, the backscattered electrons generate electron-hole pairs in quantities that depend on the energy and the intensity of the electrons. The electron–hole pairs can be partially separated by the inner electric field at the p-n junction. By passing the p- and the n-type parts through an amplifier, an output signal can be obtained which is proportional to the backscattered electrons reaching the detector. By suitably coupling the signal outputs from different diodes, one can generate both topography-sensitive as well as material-specific signals (Sect. 4.4.2).

4.3.4 Signal Display and Magnification

The signals obtained by the detectors are simultaneously displayed on a monitor. Data representation can be achieved through either analogue signal processing on a CRT (as in the older generations of SEMs) or by digitisation after displaying the data with the aid of a computer. When the first option is used, the images should be obtained via photographic techniques. The digital technique offers the chance to obtain the sample information directly, as a digital image which can be saved, modified and transferred instantly in electronic form. Both of the imaging techniques have one feature in common: the surface scanning and the representation of the surface information on the display take place simultaneously, such that each specimen point corresponds geometrically to the identical location on the recorded SEM image.

The magnification in an SEM is the ratio of the lateral length of the image displayed or printed to that of the scanned area!

This definition makes it clear that the magnification always depends on how the information is presented. For example, an SEM micrograph of 10 cm × 6 cm with 20 000× magnification has double magnification as when the picture is presented in a 5 cm × 3 cm format. Therefore, it is usual to introduce a scale bar to an image calibrated by the microscope, which automatically appears in the SEM images. Otherwise a scale bar (also called a μ-marker) must be manually marked onto a micrograph.

The reasonable magnification of SEM (M_r) is determined by the resolving power of the resolving power of the human eye (m, ca. 0.1 mm) and the resolving power of

the microscope (r). The latter depends on the signal used (e.g. SE, BSE, X-rays) and corresponds to the lateral diameter of the generation volume of the electron beam interaction product which contributes to the signal.

$$M_r = \frac{m}{r} . \tag{4.7}$$

The above statement means that the operator must calculate the upper limit of magnification using Eq. 4.7 before beginning the work. For instance, to compare an SE image with X-ray mapping, it is important to be aware that the SE image can be constructed from more pixels than X-ray mapping because the effective probe diameter for SE is on the order of 1–5 nm, whereas the X-ray probe diameter is in the order of several microns (µm), and also depends strongly on the acceleration voltage. Nevertheless, it makes sense to work with so-called empty magnifications, e.g. during X-ray point analysis. If one works with very high magnifications (for instance 500 000-fold conforms approximately to a point analysis), it is possible to observe the beam stability on the screen during the analysis.

4.4 Contrast Formation and Charging Effects

4.4.1 Secondary Electron Contrast

As already discussed in Sect. 4.2.5, PEs interact with the sample in an elastic or an inelastic manner. During the diffusion of the PEs, one or more of the processes discussed in the above section may take place. It is common to employ Monte Carlo simulation in order to obtain a statistical picture of the movement of the PEs. Figure 4.11 presents, for instance, typical path simulations for a light element (carbon) and a heavy metal (gold). For the lighter element and for high PE energies, the presence of a pear-shaped path distribution is typical. For heavy metals with lower PE energies, the distribution assumes a shape similar to that of a sectioned sphere. As a result, the penetration depth of the PEs for a lighter element is higher than that observed for a heavier one. SEs are generated during the diffusion of the PEs, but possess only a small amount of energy. Thus only the SEs produced by the surface layers can leave the surface and reach the detector. The SE efficiency and hence the signal-to-noise ratio of the image increases due to inelastic collisions close to the surface. The SE yield for elements with high atomic number Z is greater than for materials with low atomic numbers at identical PE energies, which means that the operator can reduce beam current at high Z.

The lateral resolution power of SE imaging is affected by other factors as well as the beam diameter. Besides the dependence on the electron optics, there is also a dependence on the interaction of the PEs with the sample, because SEs will be emitted from a larger region of the specimen. In particular, for light elements (such as those present in plastics), a considerable number of secondary electrons are produced far from the location of PE incidence, which ultimately deteriorate the lateral resolution. The resolution can be improved in such cases by coating a thin film of

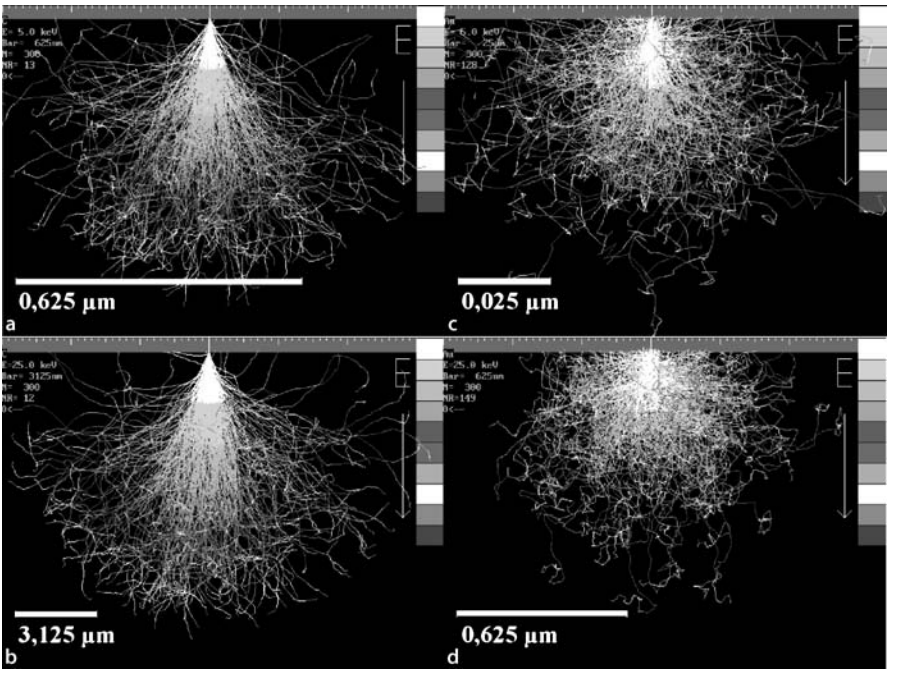

Fig. 4.11a–d. Monte Carlo simulations of the PE paths for carbon (C) and gold (Au) at different PE energies (E_P): **a** C, E_P = 5 keV; **b** C, E_P = 25 keV; **c** Au, E_P = 5 keV; **d** Au, E_P = 25 keV

heavy metal onto the sample surface. Such a coating also contributes to reducing the surface charging (see Sect. 4.4.3). The improvement results from the corresponding interactions of the PEs with the heavy metal layer. At the same time, more SEs are produced near the primary beam zone, which improves the signal-noise ratio.

The details of the SE emission determine the contrast in a SE image. Generally, good contrast is generated when the atomic number (and therefore the density) of the constituents differ significantly (see Fig. 4.12).

In polymeric materials, this kind of contrast (i.e. which depends on the atomic number) cannot be expected. The contrast formation in the SE mode is mainly determined by the local inclination of the sample surface with respect to the incident beam. This phenomenon, which is particularly apparent at surface edges (the so-called "edge effect") can be explained by the correlation between the surface and the interaction volume of the PE, as represented in Fig. 4.13. If the sample surface is not ideally flat, the interaction volume of the PE electron can pass through the side of the step, and from that location an additional number of secondary electrons can leave the sample surface, resulting in a higher SE signal. The maximum contrast enhancement occurs when the average penetration depth of the PE corresponds to the height of a step. Therefore, it can be deduced that the contrast in SEM imaging is determined not only by the atomic numbers of the elements but also the energy of the PEs selected for the SEM operation. Thus, to optimise the contrast, it is advisable not

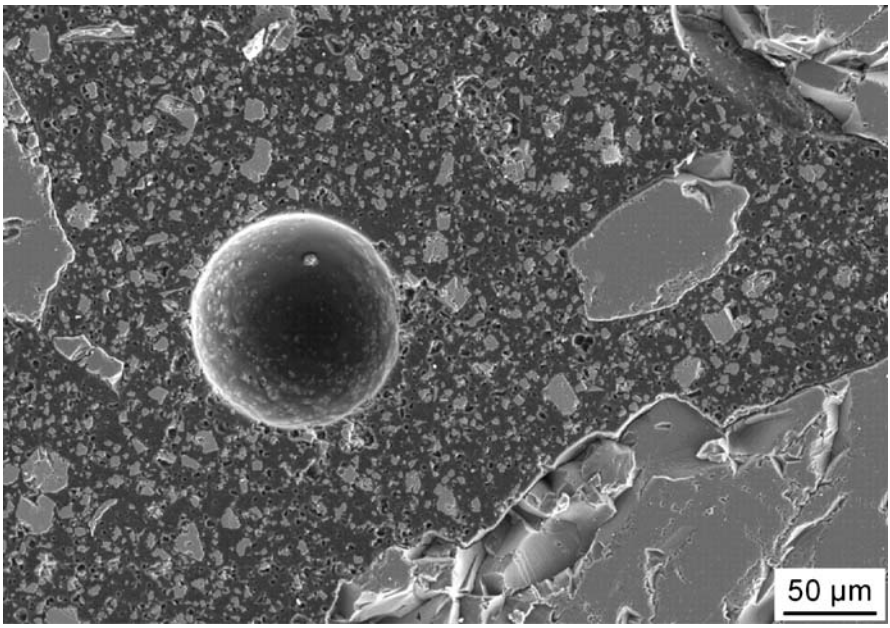

Fig. 4.12. Atomic number contrast in SE mode of a polymeric concrete sample consisting of epoxy, quartz (SiO_2, large particles), calcite ($CaCO_3$, small particles) and spherical pores

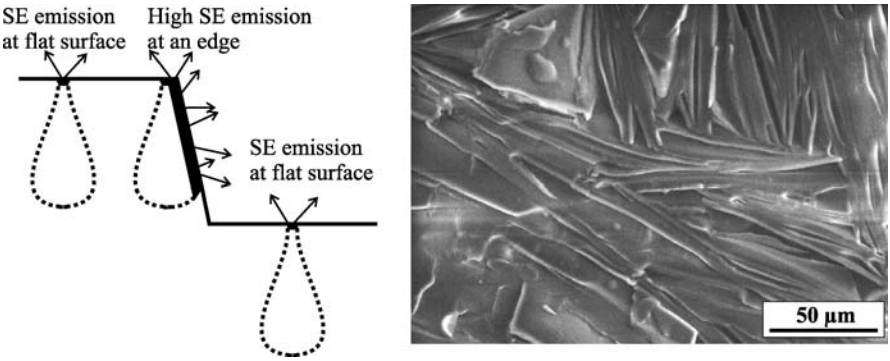

Fig. 4.13. Contrast formation in secondary electron mode due to surface relief (*right*: SE micrograph of paraffin crystals, 12 keV)

only to work at a fixed acceleration voltage, but to vary it in order to match it to the sample.

As well as a positive edge effect, a negative one can also occur; this is caused by the shadowing of SEs by the edge, and it results in a decreased SE signal.

4.4.2 Contrast of Backscattered Electrons (Solid State Detector)

The emission of the BSE can also be explained by the simulation scheme presented in Fig. 4.11. Due to the strong interactions of the PEs and the resulting lower penetration depths for elements with higher atomic numbers, these elements offer a greater probability of BSE emission. On the other hand, only BSEs that reach the detector can contribute to the signal.

The influences of the atomic numbers of the atoms within the region of interest and the surface topography on the signal detected by the individual segments (A and B) of a split BSE detector are illustrated in Fig. 4.14. By forming a sum signal (A+B) and a difference signal (A−B) of the signals A and B measured by the detector segments, the influences of the kind of material and the surface topography can be distinguished. Compositional contrasts are produced by the sum signal (A+B), while the difference signal (A−B) results from shadowing effects of the surface relief and therefore provides an impression of the sample topography.

Indeed, one should note that the efficiency of the BSEs is much lower than that of the SEs. Additionally, the noise levels of the detection and amplification systems significantly worsen the image quality when working with small beam currents in the BSE mode. In particular, the noise affects the difference signal (topography signal) of the split detector.

Furthermore, it should be noted that BSEs from a surface region corresponding to the lateral extension of the interaction volume actually contribute to the BSE signal detected, while in the case of SE detection the signal mainly results from SEs emitted from the small area where the PEs meet the sample surface.

4.4.3 Charging Effect

Both the secondary electron yield (ratio of the SEs emitted to the PEs that strike the sample) and the backscattering coefficient (the ratio of the BSEs emitted to the PEs that strike the sample) depend on the PE energy as well as the atomic number of the material and the angle of incidence of the PE [15]. Therefore, the charge supplied to the sample by incident PEs will generally differ from the charge release caused by the emission of SEs and BSEs. In most cases for bulk specimens, at PE energies of between several hundred eV and about 2 keV, the number of electrons that leave the sample exceeds the number of incident PEs, while at PE energies in the usual range (5–25 keV) the opposite is true. Consequently, the charging of insulating samples occurs (Fig. 4.15) apart from when the PE energy falls within a small range around 2 keV, where dynamic charge compensation takes place. For electrically conductive materials, the charge difference is compensated for by connecting the sample to the ground potential. To avoid the surface charging of insulating samples, their surfaces are usually coated with conducting layers of gold (Au) or carbon (C). However, it is important that the layer has sufficient contact with the specimen support held at ground potential.

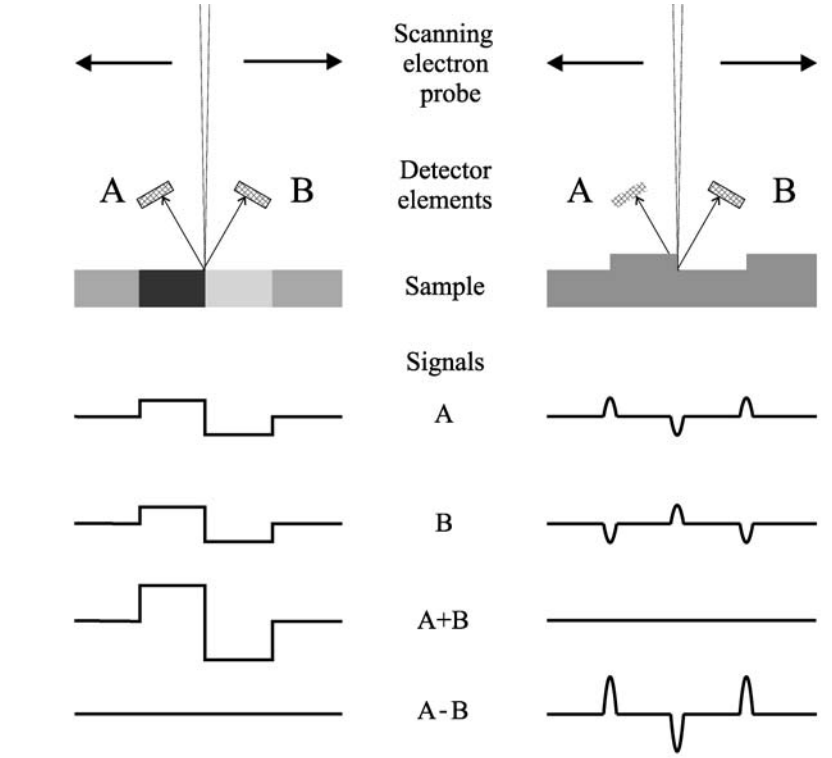

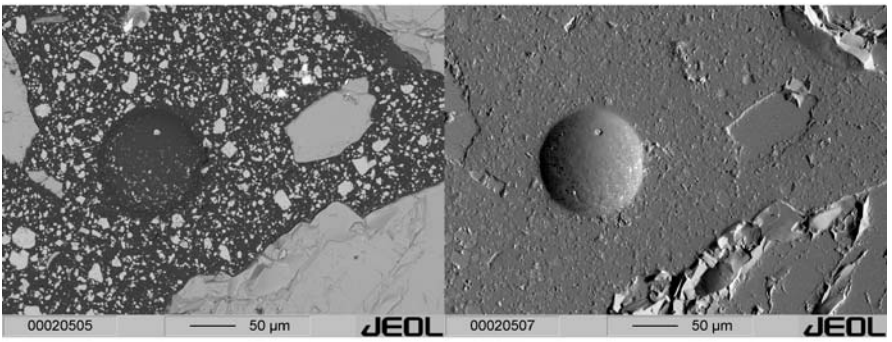

A+B = Composition A-B = Topography

Fig. 4.14. Demonstration of composition and topography contrast in BSE mode using two symmetric solid state detectors A and B (sample as in Fig. 4.12)

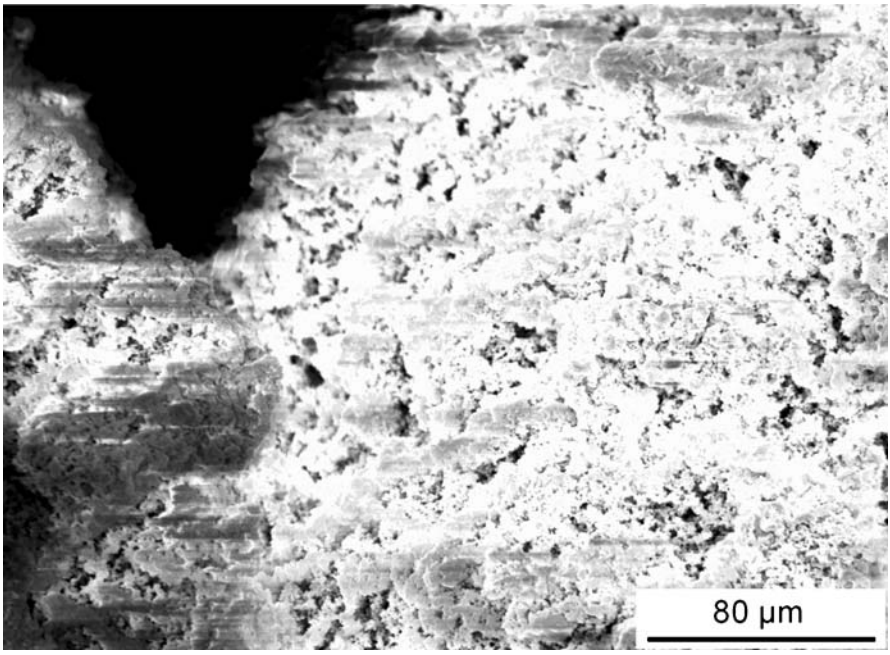

Fig. 4.15. SE image showing charging effect (porous UHMWPE reactor grains, 10 keV)

4.5 X-Ray Microanalysis

4.5.1 Physical Fundamentals of the Generation of X-Rays

The imaging of surface structures (topography) or compositional variations on the surface is sometimes insufficient to fully characterise the specimen. If, for instance, inorganic particles are embedded in a polymer matrix, X-ray microanalysis [16–19] can be useful for accurately determining the nature of these particles. So-called "characteristic" X-rays are generated by inelastic interactions of incident primary electrons with the orbital electrons of specimen atoms, as already mentioned in Sect. 4.2.5.

Orbitals, which represent the spatial probability distributions of electrons, are defined by quantum numbers. According to Pauli's exclusion principle, only one electron can have a given set of quantum numbers. The principal quantum number is the main influence on the binding energy and the distance between the nucleus and the orbital electron. The inner shells, designated K, L, M, etc., correspond to principal quantum numbers of 1, 2, 3 . . . , respectively. The other quantum numbers have a relatively small effect on the energy and cause the shells (other than the K shell) to be split into subshells.

If a localised electron is knocked out of an atom due to its interaction with a PE, the atom enters an excited high-energy state. At some later time, the empty electron orbital will be filled and the atom will relax, releasing the excess energy as a secondary effect either through the emission of a photon or alternatively through the

emission of an Auger electron (see Fig. 4.7). If the vacant electron state is an outer state, then the excess energy will be small and the emitted photon will be in the visible wavelength range (cathodoluminescence). If, however, the vacant orbital is an inner one, the amount of energy released is greater, giving rise to the emission of an X-ray photon. The atomic states that are relevant to characteristic X-ray production can be represented as horizontal lines on an energy diagram, as shown in Fig. 4.16. The energy of the emitted X-ray photon is equal to the difference between the two excited energy states (the original one of the vacant orbital and the final one of the orbital from which the electron jumps). However, it should be noted that not all transitions are allowed by the rules of quantum theory. The X-rays generated by transitions from any higher energy levels to lower K, L, or M shells are denoted K, L and M radiations, respectively. In the usual system of line nomenclature, the Greek letters α, β and γ refer to groups of lines with similar wavelengths, in order of decreasing intensity, while numerical subscripts distinguish the lines within each group, also in order of decreasing intensity. For instance, a transition from the L3 subshell to the K shell results in a $K_{\alpha 1}$ X-ray photon, while a $K_{\beta 1}$ X-ray photon is emitted by the transition from the M3 level to the K level. Further, it should be noted that the transition probability that leads to X-ray emission decreases with increasing distance between the energy levels taking part in the transition. As a result, for example, the intensity of the K_α X-ray peak is always higher than the corresponding K_β emission peak.

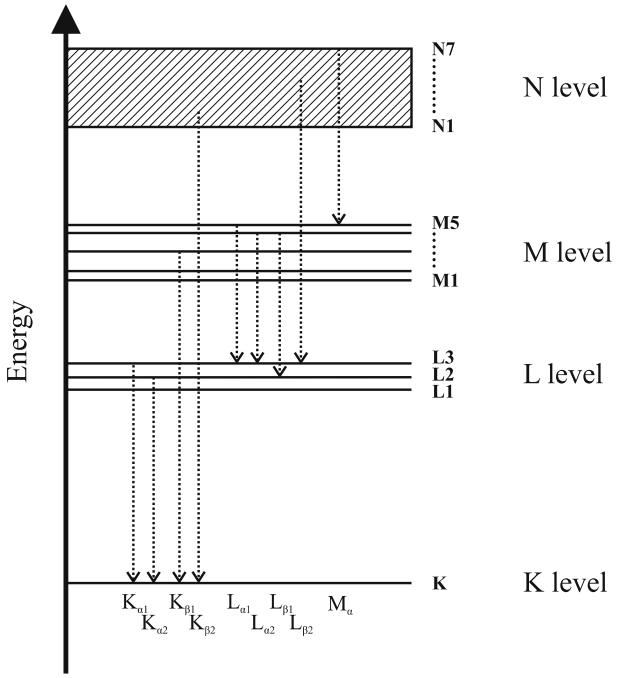

Fig. 4.16. Energy levels and possible electron transitions for the emission of characteristic X-rays (after [15, 18])

Table 4.1. Characteristic X-ray peaks of elements occurring in polymeric materials [20]

Element	K_α peak	$K_{\beta 1}$ peak	$L_{\alpha 1}$ peak	$L_{\beta 1}$ peak	M_α peak
C	0.277 keV				
N	0.392 keV				
O	0.525 keV				
F	0.677 keV				
Si	1.739 keV	1.829 keV			
Ca	3.690 keV	4.012 keV	0.341 keV		
Au			9.712 keV	11.440 keV	2.120 keV
Ti			10.267 keV	12.211 keV	2.268 keV

The energy of the characteristic radiation within a given series of lines varies monotonically with atomic number, i.e. the emitted radiation is element-specific. Therefore, for a qualitative chemical analysis, if the energy of a given K, L or M line is measured, the atomic number of the element that produces that line can be determined. Frequently observed characteristic X-ray emission peaks of elements commonly present in polymers are listed in Table 4.1.

Generally, the ionisation energy needed to excite an atom before the emission of a corresponding X-ray photon will take place exceeds the energy of the released photon. In practice, a rule of thumb is that optimal ionisation conditions are found when the energy of the incident PEs is about 2.5 times higher than that of the X-rays of interest.

X-ray emission in SEM takes place in the whole interaction volume of PE with the sample (see Fig. 4.11). Therefore, the lateral resolution of X-ray microanalysis is comparable to that of the BSE signals (see Sect. 4.4.2).

As well as the characteristic (i.e. element-specific) X-rays generated, nonspecific radiation (called "bremsstrahlung" or X-ray continuum radiation) is emitted over the same energy range. The latter results from Coulomb interactions of PEs along their paths through inhomogeneous electric fields of sample atoms. Bremsstrahlung produces a continuous spectrum with the primary electron energy as the upper limit (this corresponds to the lowest value $\lambda_{\min}$ in terms of wavelength; see Sect. 4.5.6). The contribution from bremsstrahlung must be removed from the measured X-ray spectrum to attain element-specific information. The superpositions of characteristic peaks and continuum radiation on the X-ray spectrum are shown in Fig. 4.17.

4.5.2 X-Ray Microanalysis Techniques

Two different experimental methods for X-ray microanalysis have been developed depending on the measuring technique applied:

- Energy dispersive X-ray microanalysis (EDX)
- Wavelength dispersive X-ray microanalysis (WDX).

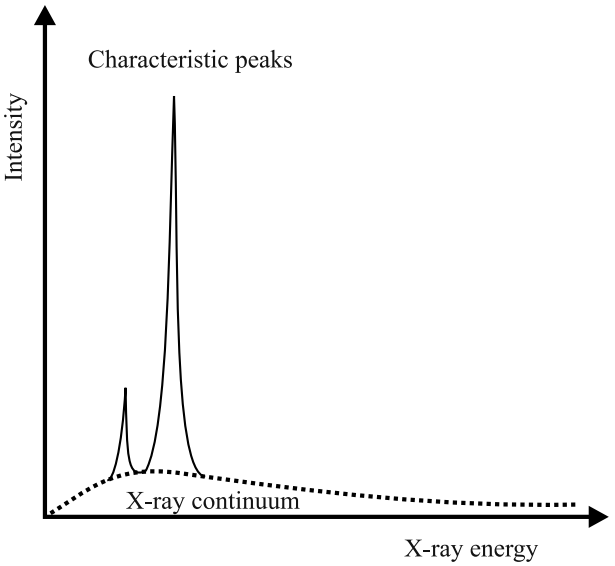

Fig. 4.17. Scheme of a typical X-ray spectrum. *Dotted line*: X-ray continuum, *solid lines*: characteristic peaks

As the names suggest, in each case the emitted X-ray will be analysed either as a function of the energy of the emitted radiation (EDX) or its wavelength (WDX). Both of these techniques are discussed briefly in the following sections.

4.5.3 Detector for EDX Analysis

EDX analysis [18–21] means energy dispersive spectroscopy of the X-rays emitted from a sample during electron irradiation. The detection technique resembles that of BSE solid state detector. X-rays penetrating the semiconductor detector are absorbed and generate electron–hole pairs. The formation of such a pair in a silicon semiconductor requires an energy of approximately 3.8 eV. Thus the number of pairs n_{eh} formed by the total absorption of the energy E_{ph} of one X-ray photon can be expressed by:

$$n_{eh} = \frac{E_{\mathrm{ph}}}{3.8\ \mathrm{eV}}\,. \tag{4.8}$$

In order to determine the number of electron–hole pairs by measuring the corresponding current pulse, it is necessary to separate the pairs using an electric field in order to stop them from immediately recombining. To achieve this, an extended (Si(Li)) region in the initially n-doped silicon detector crystal is formed using drifted lithium. The charge carriers generated in this region have sufficient lifetimes due to the dominance of intrinsic p-i-n conduction. Furthermore, the electric field required

to separate electron–hole pairs in this region is produced by applying a voltage between the outer gold contacts of the detector in such a way that the p-n junction formed at the interface between the drifted lithium region and the adjacent n-doped region is reversibly biased (see Fig. 4.18). The "separated" charges can be amplified in a field effect transistor (FET).

To stabilise lithium within the detector crystal and suppress the thermal noise of the amplifier, the detector is usually cooled with liquid nitrogen. A very thin window transparent to X-rays separates the evacuated detection unit (inside a stainless steel probe) from the atmosphere within the SEM specimen chamber, and thus prevents the cooled detector from becoming contaminated. Windows of older systems consisted mainly of beryllium, whereas in modern systems a polymer-based ultrathin window (UTW) supported by a silicon grid is used.

A sufficiently small time window is used for the basic detection cycle, during which all of the charges produced by this photon are integrated and processed to determine the energy of an individual detected X-ray photon. Using a multichannel analyser (MCA), the signal pulse is analysed based on its pulse height (which is proportional to the photon energy) and recorded as a count in the corresponding energy channel where all of these counts are accumulated. When the contents of the MCA channels are read out, an energy spectrum that shows how the accumulated counts of the channels (ordinate of the graph) depend on the corresponding photon energy (abscissa) is obtained, as demonstrated in Figure 4.19 for the spectrum of calcite.

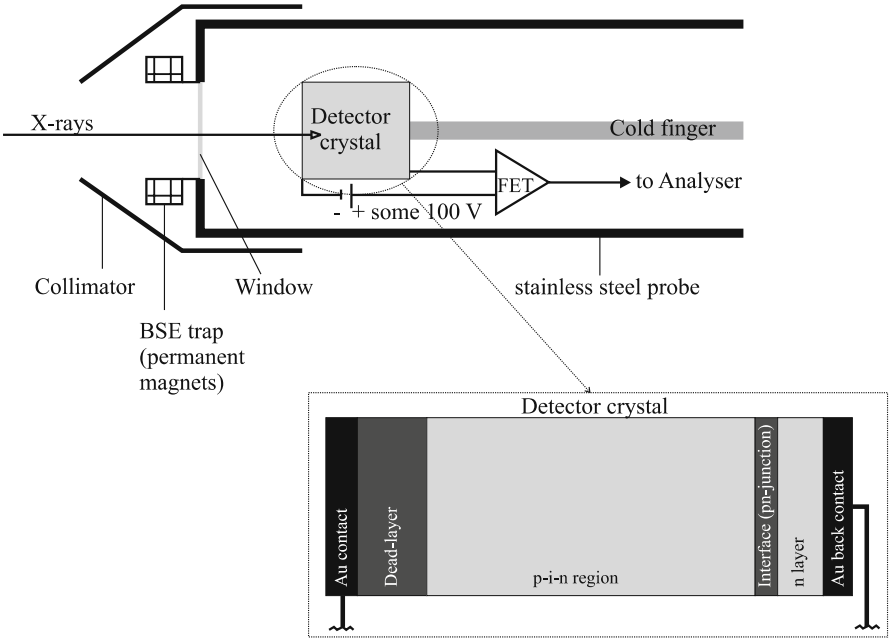

Fig. 4.18. Scheme showing the working principle of an energy dispersive X-ray detector

In order to properly evaluate the resulting X-ray spectrum, different detector specific influences should be taken into account:

1. The window and the gold layer absorb low-energy X-rays. If a beryllium window is used, only a spectrum beginning with the K_α rays for sodium (Na) can be recorded. A polymer-based UTW enables the detection of photon energies down to the K_α radiation of boron (B); however, absorption effects are significant in this low-energy region. Below 1 keV, the transparency of UTW is energy-dependent, which might lead to "virtual" peak shifts and has to be taken into account for quantitative considerations.
2. Between the gold electrode and the p-i-n region is a dead layer in which the electron–hole pairs can immediately recombine. X-ray photons with penetration depths that do not exceed the thickness of the gold contact and the dead layer cannot contribute to the signal.
3. If the X-ray energy of a photon is high enough that it can penetrate into the *n*-conducting region of the detector, electron–hole pairs that form in this part of detector do not contribute to the signal either. Therefore, the energy determined is too low, resulting in a loss of intensity at the actual energy of the photon and increased intensity at lower (falsely determined) energy.
4. The value of 3.8 eV mentioned as the energy needed to produce an electron–hole pair in Si(Li) is only an average value. Actually, there are a wide range of energies, so different numbers of electron–hole pairs can be generated for the same X-ray energy. This causes the peaks in the MCA to broaden, and this deviation increases with increasing X-ray energy. Peak broadening can lead to the overlapping of neighbouring peaks.
   The measured full width at half maximum (FWHM) of the K_α radiation of manganese (Mn) is usually used as the energy resolution when evaluating the quality of a detector. Good Si(Li) detectors possess energy resolutions of smaller than 130 eV.

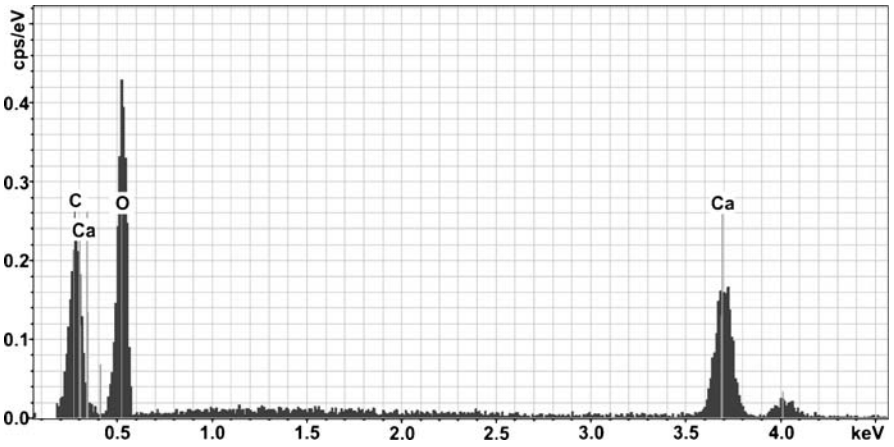

Fig. 4.19. EDX spectrum taken from a small particle (calcite, $CaCO_3$) in Fig. 4.12

5. X-ray absorption in the detector does not exclusively result in the formation of electron–hole pairs; it can also cause fluorescence emission from silicon (escape peak).

Consequently, peak heights are strongly influenced by measuring conditions and will not directly yield quantitative information on local concentrations of elements.

EDX detectors with take-off angles of between 35° and 45° are usually used. To increase the detection efficiency, the acceptance angle of the detector should be as high as possible, i.e. the detector must be placed very close to the sample. Furthermore, we must take into consideration that the X-rays to be detected should not be blocked by preceding surface structures on the sample. Therefore, the EDX analysis of a sample with a rough topography can be difficult.

Compared to integral element analysis methods, the sensitivity of EDX analysis is relatively low; however, it provides the ability to carry out a microanalysis within an interaction volume that is in the micron or even submicron range. A limit of detectability (in terms of concentration) of about 0.1 wt% holds for elements of medium and high atomic numbers, while elements with low atomic numbers need a concentration of more than 1 wt% to be detected.

4.5.4 Quantitative EDX Analysis

Quantitative EDX analysis [18–23] plays only a secondary role in polymer research. The reason for this is that the polymers are generally composed of the light elements carbon and hydrogen, with higher atomic number elements being present, if at all, only in very small amounts (generally below the detection limit; Sect. 4.5.3). Also, for polymers containing additives, the actual excitation volume of the additives is usually too small. The material in and around the excitation volume must be homogeneous. This requirement is usually not fulfilled by heterogeneous polymers containing relatively small particles. Additionally, a very flat surface is essential for a quantitative analysis. Therefore, only a short description of quantitative microanalysis will be presented here. As well as detector-specific properties, one should take also into account the X-ray emission in the excitation volume and the path of the photons in the material.

Initially, a qualitative analysis must be carried out. As absorption and fluorescence take place in the detector itself, the silicon escape peak should be subtracted from the spectrum. The spectrum obtained after this step is subjected to peak separation (separation of overlapping peaks) and then the peaks are fitted with Gaussian functions. Then the X-ray continuum for all of the elements present is calculated and will be subtracted. Finally, the intensity under each Gaussian peak is integrated. This results in intensity values for each peak. Two methods can then be applied: K ratios or ZAF correction.

K Ratios

If the intensity values of the peaks of standard elements recorded under equal conditions are known, then quantitative analysis can be conducted relatively easily. To

do this, one constructs the so-called K ratio, which is the ratio of the measured peak intensity to the intensity of the standard sample peak. The result is, however, only a first approximation, because the real ratio corresponding to the absorption and fluorescence is not taken into account in this procedure.

ZAF Correction

Correction factors corresponding to the atomic number (Z), absorption (A) and fluorescence (F) are introduced in order to achieve an improved quantitative analysis. The Z term contains both the backscatter coefficients and the stopping power needed for the generation of an X-ray continuum.

X-ray photons emitted in the interaction volume can be absorbed (A term) along their paths through the specimen. On the other hand, absorbed radiation can also initiate the emission of fluorescence radiation with lower energy (F term).

Intensity values obtained and processed in this way can be used to conduct a quantitative analysis that considers all parameters. Comparisons with real standard samples (analysis with standards) or with virtual standards (standardless analysis) are made, whereas proportions of known elements that are not measurable can be calculated by a subtractive method.

If the sample thickness is smaller than the excitation volume for the X-ray radiation (as is the case for ultrathin sections), this fact should also be taken into account.

Manufacturers also deliver microanalysis systems with corresponding software that also take into account instrumental parameters for quantitative evaluations. During individual steps correction and calculation steps, it is also possible to carry out manipulations in an interactive way that minimises errors. In particular, when the specimen is not prepared as required for systematic studies (i.e. flat surface, homogeneous material, etc.), one should check the results for plausibility (e.g. the stoichiometry, see the discrepancy in quantitative results in Fig. 4.20 for SiO_2).

4.5.5 X-Ray Mapping

The SEM provides, beside the integral analysis discussed above (Sects. 4.5.1 and 4.5.2), the ability to determine the elemental distribution (elemental mapping) over a sample surface. To do this, in an EDX system one or more peaks from an interesting element are selected from the spectrum by so-called regions of interest (ROI). While scanning the electron beam, it is possible to record the X-ray counts of the ROI correlating to points on the specimen surface. By accumulating X-ray counts per pixel, it is possible to create an elemental distribution image (X-ray mapping, see Fig. 4.21).

4.5.6 Wavelength Dispersive X-Ray Microanalysis (WDX)

WDX microanalysis [16, 22] was the original method used for elemental analysis by electron-induced X-ray emission. However, due to the time-consuming nature of this method, this technique is currently employed only when high spectral resolution is required (5–20 eV), or element concentrations of less than 0.1wt% need to be measured.

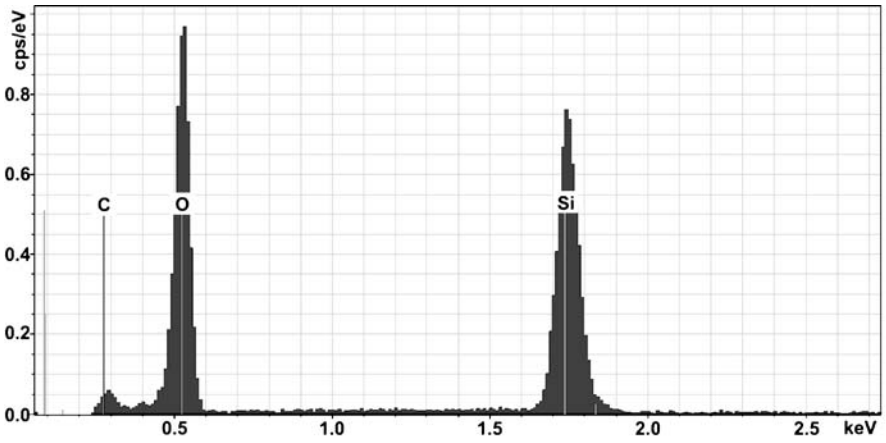

Quantitative EDX-analysis via ZAF correction

element	series	[weight-%]	[norm. weight-%]	[norm. at.-%]	error in %
silicon	K-series	37,390073	36,06903212	24,32263978	1,586829093
oxygen	K-series	66,27246187	63,93096788	75,67736022	8,579591982
	sum:	103,6625349	100	100	

Fig. 4.20. EDX spectrum taken from a large particle (quartz, SiO_2) in Fig. 4.12 and its quantitative (ZAF) results; C peak results from coating used to prevent charging

The relationship between the energy E and the wavelength λ of an X-ray photon is given by Planck's relation:

$$E = h\nu = h\frac{c}{\lambda} \tag{4.9}$$

where ν denotes the frequency of radiation, $h = 6.6260755 \times 10^{-34}$ Js is Planck's constant, and c is the velocity of light in vacuum.

For WDX analysis, the diffraction of X-rays by a crystal lattice is used to discriminate X-rays according to photon wavelength. Diffraction is an interference phenomenon, where intensity maxima only occur when the path differences between the waves diffracted in the same direction correspond to integer values n of the wavelength λ. Consequently, diffraction takes the form of a reflection of the incident beam at lattice planes, as illustrated in Fig. 4.22. The relation between the glancing angle θ, the inter-planar distance d of the lattice planes and the wavelength λ is given by Bragg's law:

$$n\lambda = 2d \sin\theta\,. \tag{4.10}$$

Thus, the incident X-ray beam can be monochromatized by using an appropriately selected inter-planar distance d, and the wavelength of the monochromatized beam can be changed by varying the glancing angle.

The WDX monochromator system comprises a crystal with a suitable value of d, an X-ray detector (a gas proportional counter) and a slit in front of it. The positions

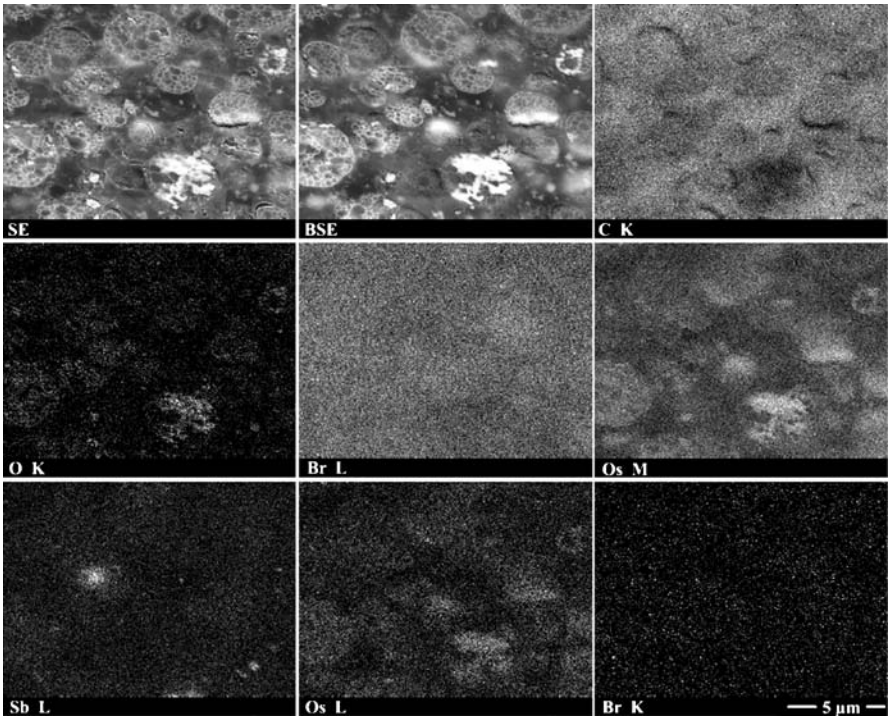

Fig. 4.21. SE image, BSE image and X-ray mapping of C, O, Br, Os, Sb (cut surface for TEM preparation of flame-retarded HIPS with OsO_4 staining)

of the sample, crystal and detector are arranged in such a way that the glancing angle of the radiation incident on the crystal and that of the radiation diffracted towards the detector slit are identical (see Fig. 4.23). This condition is fulfilled only when the sample, the crystal and the detector are positioned on a circle called a Rowland circle. When the arrangement shown in Fig. 4.23 is used, the detector measures the X-ray intensity of the wavelength λ filtered according to Eq. 4.10 (usually for $n = 1$) from the radiation striking the monochromator crystal, where the wavelength selected is

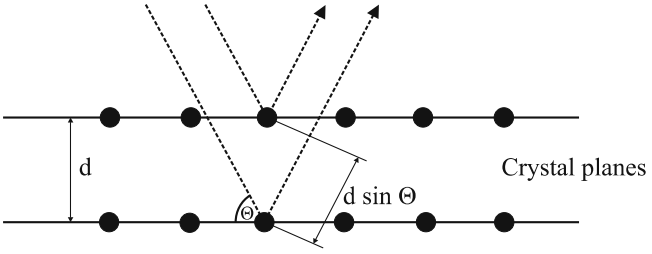

Fig. 4.22. Interference scheme for X-rays diffracted on crystal planes (Bragg's law)

determined by the glancing angle used. Therefore, to record a wavelength-dispersive spectrum, the sample position is kept fixed and the glancing angle is varied by shifting both the monochromator crystal and the detector along the Rowland circle to the position needed.

In order to make use of not only the central part but an extended region of the crystal in order to monochromatize the incident radiation, the crystal is concavely bent to a radius of curvature which is twice that of the Rowland circle and then ground in such a way that its surface has a radius of curvature equal to that of the Rowland circle. Such a spectrometer is known as Johnsson fully focussing spectrometer.

When only one individual crystal (i.e. only one value of d) is used, the measurable wavelength range is limited for technical reasons. Therefore, WDX systems are often equipped with several monochromator crystals with different d values, as shown in Table 4.2.

The measuring conditions for WDX analysis require the exact positioning of the region of interest on the sample surface at the point of intersection of the electron optical axis with the Rowland circle. The adjustment is usually carried out with the help of an optical microscope attached to the SEM.

Compared to EDX microanalysis, WDX analysis possesses a relatively poor signal-to-noise ratio and requires a higher electron beam current. This method is therefore not suited to use as a routine analytical technique for polymers due to the risk of beam damage. When it is used for quantitative analysis, the effects described in Sect. 4.5.4 should be taken into account.

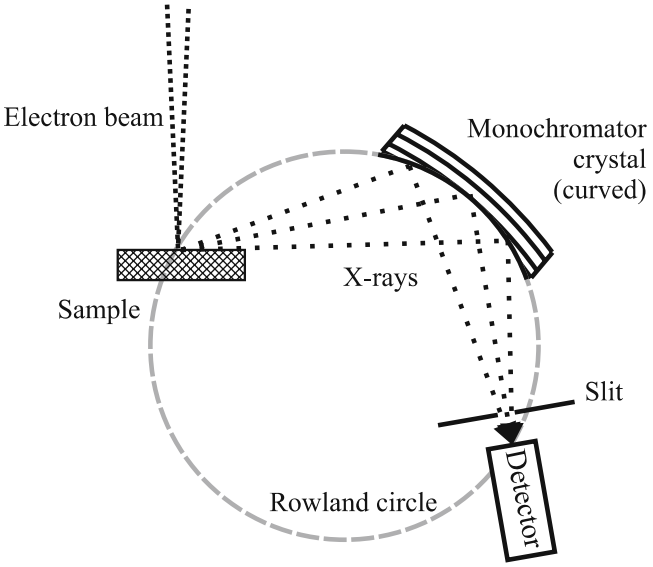

Fig. 4.23. Scheme of a Johnsson fully focussing wavelength dispersive spectrometer: specimen, crystal and detector are arranged on the Rowland circle

Table 4.2. Different types of monochromator crystals commonly used in WDX spectrometers

Crystal	2*d* spacing of specific planes used (nm)	Region of detectable wavelength (nm)	Minimal detectable atomic number
LiF	0.40	0.08–0.4	19
α-Quartz	0.67	0.12–0.6	15
Pentanerythritol (PET)	0.87	0.15–0.8	13
Rubidium acid phthalate (RAP)	2.61	0.5–2.4	8
Potassium acid phthalate (KAP)	2.66	0.5–2.4	8
Pb stearate	10.4	2.0–9.0	5

4.6 Environmental Scanning Electron Microscope (ESEM™)

4.6.1 Low-Vacuum SEM and ESEM™

The environmental scanning electron microscope (abbreviated to ESEM) is a modified SEM that offers new applications and advantages over the conventional SEM, as described in more detail in Sects. 4.6.2 and 4.6.3.

Used in this context, the term "environmental" refers to the possibility of imaging wet samples such as biological samples using the SEM.

The ESEM was developed in the 1980s. At that time, many SEM manufacturers introduced scanning microscopes that had low vacuums of about 10^{-1} mbar in their specimen chambers, which were achieved using a special pumping system. In these low-vacuum SEMs, charging effects can be strongly reduced and hence isolated samples can be imaged without coatings.

Unfortunately, an Everhardt-Thornley detector (see Sect. 4.3.3) cannot be used in a low-vacuum SEM, as electrical breakdown at the high-voltage part of the detector cannot be avoided. Therefore, most producers of low-vacuum SEMs only have used BSEs to image the sample surface, which of course leads to limitations on the lateral resolution, as described in Sect. 4.4.2. Danilatos and coworkers developed and patented [24] a relatively simple SE detection system for a vacuum exceeding 1 mbar, which found application in a microscope called an ESEM [25]. The first ESEMs were constructed and commercialised by the company ElectroScan. Today, "ESEM" is a trademark of FEI.

4.6.2 Avoiding Charging

As described in Sect. 4.4.3, incident PEs usually cause negative charging of the surfaces of electrically nonconducting samples. Under low-vacuum conditions, a lot of residual gas molecules are ionised by the primary electron beam. The resulting positive ions are attracted by the negatively charged sample surface, and so the surface charge is compensated for by the impacting ions. Therefore, the surface charging of insulating samples is avoided or strongly reduced in a low-vacuum SEM. The presence of an additional electric field, as used in a "gaseous secondary electron detector"

(see Sect. 4.6.4) can further enhance this effect, because more ions are formed by cascade ionisation, which are then available for neutralisation of the surface charge.

4.6.3 The Wet Mode

The ability of an ESEM to investigate wet samples is of great practical importance. Specimens do need not to be dried before the investigation, and they are not dried during the investigation either, as the pressure in the specimen chamber of the ESEM is comparable with the partial vapour pressure of water at room temperature. By using a differential pumping system [26], which involves introducing some diaphragms to separate regions with different levels of vacuum along the electron-optical axis from one another, an ESEM can work with a relatively high pressure in the specimen chamber while a high vacuum or even an ultrahigh vacuum is utilised in the microscope column and the electron gun. The maximum pressure achieved in the specimen chamber depends on the diameter selected for the last diaphragm of the pressure system. A smaller one must be selected to maintain a high vacuum in the column at increased pressure in the specimen chamber. A small diaphragm, however, affects the field of vision, especially at lower magnifications and lower working distances.

In the so-called "wet mode", the previously evacuated sample chamber is vented to a pressure of some mbar of water vapour, so that, to a good approximation, only water molecules are present in the chamber. Depending on the microscope type, the maximum achievable pressure can range from less than 1 mbar to 15 mbar.

Figure 4.24 shows the phase diagram of water close to its triple point. One can see that the transition from the liquid state to the gas phase at room temperature occurs at a pressure of 28 mbar. Therefore, if the water vapour pressure inside the sample chamber is 28 mbar and if the sample contains water, there will be a thermodynamic equilibrium. Under these conditions, the sample does not lose water by boiling and

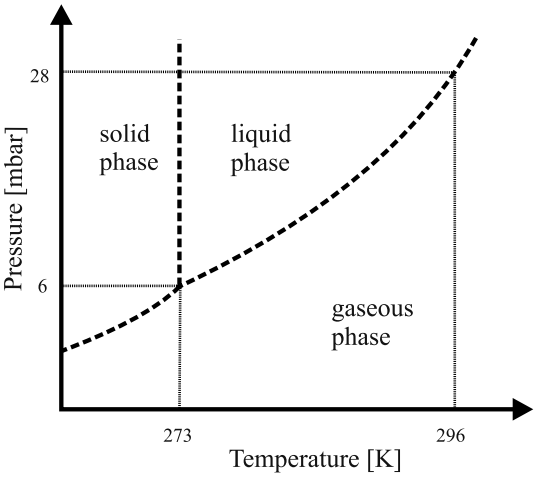

Fig. 4.24. Scheme of the phase diagram of water in the range usable in ESEM

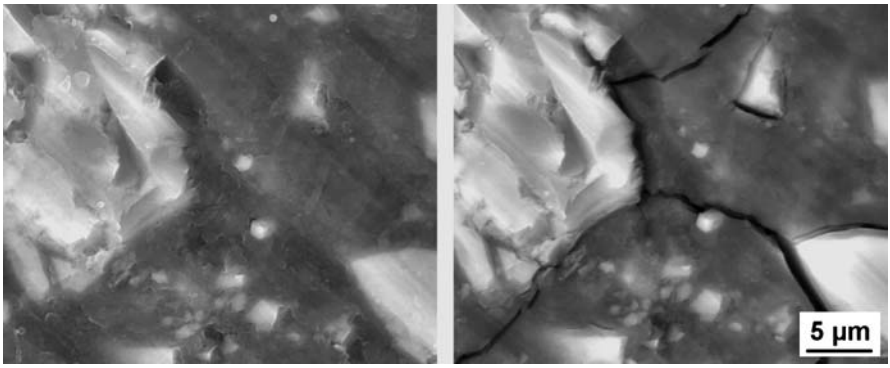

Fig. 4.25. ESEM (GSED) micrographs of a hydrated dental composite. *Left*: ambient conditions 7 mbar and 277 K. *Right*: after drying at lower pressure (3 mbar, 277 K)

a film of water is not deposited onto the sample surface. Upon increasing the pressure, the specimen will be covered with a film of water, while decreasing the pressure causes the sample to dry out. When working with an ESEM equipped with a FEG, one cannot create a pressure of 28 mbar, but one can shift the working conditions along the liquid/gas phase transition towards the lower pressure region by cooling the sample, e.g. by means of Peltier cooling.

The wet mode is the standard working mode of the ESEM. Water vapour can be produced without difficulty using distilled water. The water in the atmosphere also forms enough ions to eliminate surface charging. Therefore, this mode is ideal for water-containing samples as well as for imaging nonconducting polymeric materials without coatings. It is also a highly advantageous approach to use for in situ investigations of polymers. Besides micromechanical tests, special investigations involving variations in temperature, pressure or the use of a particular gas atmosphere can be carried out using this technique (see Chap. 6, Fig. 6.1). The reactions of the sample with gas molecules and the adhesion properties of its surface can also be comfortably studied using ESEM.

Figure 4.25 shows the effect of the surrounding atmosphere on SE imaging in the case of a hydrated dental composite sample. When imaging in wet mode (with the surrounding atmosphere at close to the partial pressure of saturated water vapour), sample drying can be reduced and the formation of cracks is avoided (left). When imaging at lower pressures, vacuum water is removed from the sample, so that cracks appear at the interface to the glass ceramic particles (right).

If it is impossible to use the water vapour pressure for practical reasons, the ESEM can also be operated under other gases. If, for example, nitrogen gas is used, charging effects can also be suppressed and SE imaging can be achieved using the GSED (see below).

4.6.4 The Gaseous Secondary Electron Detector (GSED)

The patented GSED [24] uses cascade ionisation of the residual gas molecules to amplify the secondary electron signal. Figure 4.26 shows the principle of this detector schematically. An isolated, positively biased electrode with a central hole, which the primary electron beam can pass through, is placed directly under the last diaphragm of the pumping system. If the operator intends to use a BSE detector at the same time, SE detection using a collection electrode that is not centrally arranged is also possible.

Secondary electrons that leave the sample surface are accelerated towards the positively biased electrode and ionise residual gas molecules along their paths to the collector. The free electrons thus generated are also forced to travel towards the collector electrode and can trigger new ionisation events. These cascade processes cause the number of originally released SEs to be multiplied enormously, resulting in a measurable current at the collector electrode, which can also be amplified electronically. The final current signal is proportional to the number of SEs emitted per unit time, and it can therefore be used to image the sample. However, it should be noted that this SE signal is also influenced by the number of residual gas molecules available for ionisation (i.e. the pressure in the specimen chamber), the ionisation probability (i.e. the type of gas molecules present), the distance and the voltage between the sample and the collector electrode.

A large working distance and a high pressure are favourable for high signal amplification. However, because of the widening of the primary electron beam due to collisions with residual gas molecules (skirt effect), highly resolved imaging (particularly at low PE energies) requires the use of a small working distance and/or a low pressure.

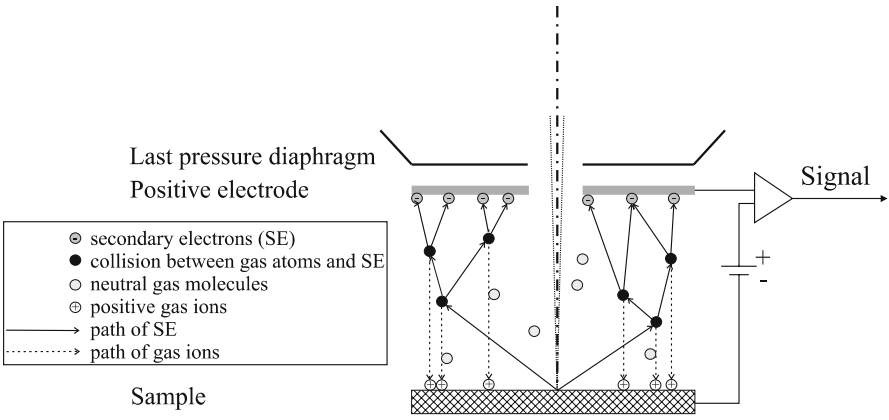

Fig. 4.26. Scheme showing the principle of the gaseous secondary electron detector (GSED)

References

1. Knoll M (1935) Z Techn Physik 16(11):467
2. Ardenne Mv (1938): Z Phys 109(9-10):553
3. Ardenne Mv (1938) Z Techn Phys 19:407
4. Ardenne Mv (1940): Elektronen-Übermikroskopie (in German). Springer, Berlin
5. Zworykin VK, Hiller J, Snyder RL (1942) ASTM Bull 117:15
6. McMullan D (1952) PhD thesis, University of Cambridge, Cambridge
7. Smith KCA (1956) PhD thesis, University of Cambridge, Cambridge
8. Everhardt TE, Thornley RFM (1960) J Sci Inst 37:246
9. Castaing R (1951) Application des sondes électroniques à une méthode d'analyse ponctuelle chimique et cristallographique. PhD thesis, University of Paris, Paris
10. Coslett VE, Duncumb P (1956). In: Sjöstrand FS, Rhodin J (eds) Proc Stockholm 11th Conf Electron Microsc. Almqvist and Wiksell, Stockholm, p 12
11. Danilatos GD (1983) Micron Microsc Acta 14(4):307
12. Danilatos GD (1985) Scanning 7:26
13. Danilatos GD (1986) In: Bailey GD (ed) Proc 44th Annual Meeting EMSA. San Francisco Press, San Francisco, CA, p 630
14. Danilatos GD (1986) In: Bailey GD (ed.) Proc 44th Annual Meeting EMSA. San Francisco Press, San Francisco, CA, p 632
15. Reimer L (1998) Scanning electron microscopy: Physics of image formation and microanalysis, 2nd edn. Springer, Berlin
16. Lee RE (1993) Scanning electron microscopy and X-ray microanalysis. PTR Prentice Hall, Englewood Cliffs, NJ
17. Goldstein JI, Newbury DE, Echlin P, Joy DC, Fiori C, Lifshin E (1981) Scanning electron microscopy and X-ray microanalysis. Plenum, New York
18. Reed SJB (1993) Electron microprobe analysis, 2nd edn. Cambridge Univ. Press, Cambridge
19. Chandler JA (1987) X-Ray microanalysis in the electron microscope. In: Glauert AM (ed) Practical methods in electron microscopy, vol 5, part II. Elsevier, Amsterdam
20. Friel JJ (1995) X-Ray and image analysis in electron microscopy. Princeton GammaTech Inc., Princeton, NJ
21. Russ JC (1984) Fundamentals of energy-dispersive X-ray analysis. Butterworths, London
22. Heinrich KFJ, Newbury DE (1991) Electron probe quantitation. Plenum, New York
23. Scott VD, Love G, Reed SJB (1995) Quantitative electron probe microanalysis, 2nd edn. Ellis Horwood, New York
24. Mancuso JF, Maxwell WB, Danilatos GD (1988) US Patent 4 785 182
25. Knowles WR, Schultz WG, Armstrong AE (1994) US Patent 5 362 964
26. Danilatos GD, Lewis GC (1989) US Patent 4 823 0062